IEEE Access
Multidisciplinary | Rapid Review | Open Access Journal

Received 19 October 2023, accepted 5 November 2023, date of publication 10 November 2023,
date of current version 15 November 2023.

Digital Object Identifier 10.1109/ACCESS.2023.3331365

TOPICAL REVIEW

Metal Oxide Coated Optical Fiber for Humidity Sensing Application: A Review

SITI NASUHA MUSTAFFA[1], AFFA ROZANA ABDUL RASHID[2], TAN SIN JIN[3], P. SUSTHITHA MENON[1], (Senior Member, IEEE), MOHD ZULHAKIMI AB RAZAK[1], ARNI MUNIRA MARKOM[4], HAZLIHAN HARIS[5], ISMAIL SAAD[5], (Senior Member, IEEE), AND AHMAD RAZIF MUHAMMAD[1]

[1]Institute of Microengineering and Nanoelectronics, Universiti Kebangsaan Malaysia (UKM), Bangi, Selangor 43600, Malaysia
[2]Faculty of Science and Technology, Universiti Sains Islam Malaysia, Nilai, Negeri Sembilan 71800, Malaysia
[3]School of Engineering, UOW Malaysia University College, Shah Alam, Selangor 40150, Malaysia
[4]School of Electrical Engineering, College of Engineering, Universiti Teknologi MARA, Shah Alam, Selangor 40150, Malaysia
[5]Faculty of Engineering, Universiti Malaysia Sabah, Kota Kinabalu, Sabah 88400, Malaysia

Corresponding authors: Affa Rozana Abdul Rashid (affarozana@usim.edu.my) and Ahmad Razif Muhammad (a.razif@ukm.edu.my)

This work was supported in part by the Ministry of Higher Education Malaysia (MOHE) under the Fundamental Research Grant Scheme (FRGS) under Grant FRGS/1/2021/TK0/UKM/02/34, and in part by UOW Malaysia University College.

ABSTRACT Humidity measurement in biomedicals, industry and electronic manufacturing applications needs an accurate and fast measurement of relative humidity by the sensor. In recent years, electronic sensors are utilized in the market, but optical humidity sensors provide several advantages over it. This paper reports the classification of optical fiber humidity sensors based on their working principles, such as fiber Bragg gratings, interferometers, and resonators. Along with the mentioned optical fiber structures, their fabrication process, equipment required for humidity sensing and the coating technique used are explained in this review. Recently, metal oxide semiconductors have been widely used as sensing material, specifically in humidity sensor applications. Thus, this paper explores optical fiber humidity sensors based on the three working principles mentioned, all of which incorporate metal oxide coatings. This review reveals that the most commonly used metal oxide for optical fiber humidity sensing is graphene oxide. This is because graphene oxide offers high sensitivity, fast response and recovery time over the other types of metal oxide. A large number of oxygen-containing groups on the surface and edge of graphene oxide also contribute to humidity sensing performance since it can permeate and absorb more water molecules. The use of hybrid nanomaterials is recently discovered and their potential as emerging coating material for optical applications are not fully exploited yet. Thus, there is still an opportunity for improvement in terms of sensitivity, response and recovery time in the context of optical fiber humidity sensor.

INDEX TERMS Metal oxide, fiber optic, humidity sensor.

I. INTRODUCTION

Humidity is an important aspect that plays a crucial role in our lives, with applications ranging from the living environment to industrial production and food storage [1], [2]. Humidity is defined as the amount of water in the atmosphere and can be measured as absolute humidity (AH) or relative humidity (RH). The contrast between these two types are based on their definition, measurement and temperature impact. The first type is absolute humidity, which is the actual amount of water vapor presents in the air, giving the ratio of the mass of water vapor to the mass of dry air. The unit for AH is in grams of moisture per cubic of air (g/m^3) and it is independent of temperature [3], [4], [5].

The second type of humidity is relative humidity (RH) which is the ratio of the amount of moisture content of air to the maximum moisture level that the air can carry, and it is highly dependent on the temperature [6], [7], [8], [9]. In this

The associate editor coordinating the review of this manuscript and approving it for publication was Chao Zuo.

study, the relative humidity sensing will be reviewed by using different types of metal oxide as sensing material for optical fiber humidity sensor (OFHS).

Humidity sensors are widely used in many applications to detect specific AH and RH values. For example, humidity monitoring in medical applications specifically monitors the air supplied to mechanically ventilated patients in critical care [10], [11]. The suitable range of AH and RH values at the level of the upper trachea is between 5 mg/L (50% RH at 27-28 °C) and 42 mg/L (85% RH at 34 °C nasal, 95% RH at 35 °C naso/orophaynx). If the AH level is lower than 5 mg/L, it indicates a high risk of respiratory complications due to insufficient humidification of inspired air [12]. Apart from biomedical applications, humidity sensors are also commonly used in cooling the computers, heat treating furnaces, smelting furnaces and clean rooms [13]. Different requirements of humidity are critical for applications mentioned above. If these conditions are not met, respiratory system of patients in critical care unit will be affected and operations may not function properly.

Over the years, many kinds of humidity sensors have been created, such as capacitive, resistive and optical humidity sensors [14], [15], [16], [17]. These days, humidity sensors available in the market comprise of electronic sensors. The optical fiber humidity sensor has more advantages than the electronic sensor due to its smaller size, higher durability, and the ability to work in inflammable environments at higher temperatures and pressure [18]. Predominantly, their electromagnetic immunity contributes to the OFHS tolerating hazardous and demanding conditions in industrial processes [19], [20], [21]. OFHS can be categorized based on their working principles, namely (1) fiber Bragg grating (FBG), (2) interferometer and (3) resonator. These sensing techniques of OFHS will be discussed in detail throughout this review.

Researchers have put in various efforts to identify the best sensing materials for optical fiber humidity sensor based on fiber optics. Recently, metal oxide semiconductors have been broadly utilized as sensing material, particularly in sensor applications. Metal oxide is made up of an oxide anion with a cation of a single metal or metalloid element [22]. The commonly used metal oxides are titanium dioxide (TiO_2), zinc oxide (ZnO), tin (IV) oxide (SnO_2) are synthesized and studied for practical applications [23]. Semiconductor metal oxides have a rich history in gas sensing, dating back to their discovery in the 1960s. There are known for their small size, cost effectiveness and compatibility with simple measuring instruments [24], [25], [26], [27], [28]. These properties have made them a popular choice for gas sensors due to their quick and sensitive detection capabilities [29], [30]. While this review primarily focuses on metal oxide coatings in humidity sensors, it is worth nothing their extensive use and development in gas sensing applications over the years.

Research conducted by Ascorbe et al. revealed that sensing performance using water-swelling materials, such as polymeric coatings and inorganic salts on the fiber, was not promising. They recorded low sensitivity, slow response and recovery times [18]. These materials also possess nonlinear behavior, especially at high relative humidity percentages, making them not compatible for humidity sensing applications. However, metal oxide coatings have shown excellent linear responses and high sensitivity within the humidity range of 20% to 90% RH, making them a suitable choice for humidity sensing. Study by Li et al. indicated that group IV metal oxide coatings, such as hafnium oxide (HfO_2), zirconium dioxide (ZrO_2), and TiO_2, demonstrated improved chemical stability and corrosion resistance [31]. These findings suggest that metal oxide coatings may be a more suitable option for optical fiber humidity sensors when compared to other materials like polyvinyl alcohol and polymethyl methacrylate. While we did not directly compare the performance of metal oxide coatings with other materials on the same fiber sensors, the literature supports the idea that metal oxide coatings offer several advantages over other materials for humidity sensing applications. Furthermore, metal oxides are more cost-effective when compared to alternative materials [28], [32], [33].

The purpose of this study is to summarize the metal oxide coating used for optical fiber humidity sensors. The second objective of this study is to identify the commonly used metal oxides as sensing materials that can help to enhance the sensor's sensitivity at low and high relative humidity. Hence, this review is structured as follows, an introduction that includes the definition of absolute and relative humidity, applications of humidity sensing, the advantage of OFHS over electronics humidity sensors, metal oxides as sensing materials for OFHS. In Section II, three different sensing techniques; (1) fiber Bragg grating (FBG), (2) interferometer and (3) resonator used in OFHS are outlined. FBG can be further classified into uniform FBG, tapered FBG, tilted FBG, long period grating and micro-nano structured FBG. Two types of interferometers and resonators are covered in this review, which encompassed Mach-Zehnder and Michelson interferometers, and microfiber knot and microfiber loop resonators. OFHS structure along with their sensing mechanisms will be elaborated in this review. Additionally, work done by others on humidity sensing with metal oxides will reviewed as well. Lastly, in Section III, the conclusion regarding this topic and recommendations for future work will be discussed.

II. CLASSIFICATION OF OPTICAL FIBER HUMIDITY SENSOR BASED ON WORKING PRINCIPLE

A. FIBER BRAGG GRATINGS (FBG)

Fiber Bragg gratings (FBG) is a common sensing method widely used for various physical parameter measurements such as pressure, strain and temperature. It is broadly used as it has many pros such as tiny in size, multiplexing capability, great sensitivity, light, and immunity to Electromagnetic Interference (EMI) [34], [35], [36], [37]. Bragg gratings are an optical structure containing periodic perturbation of the refractive index (RI) of a waveguide [38]. FBG is produced by exposing the core of the fiber to intense laser light with a

periodic pattern and this will permanently raise the refractive index of the core. Grating is the fixed index modulation and has a period reliant on the exposure pattern [39], [40]. FBG permits the transmission of some wavelengths and reflects others, as depicted in Fig. 1. This behavior is analogous to the wavelength peak of the FBG, which corresponds to its characteristic period. In humidity sensing applications, FBG sensor as a sensing technique is common since many research studies are focused on this technique. In this following section, five types of FBGs are discussed, along with their sensing mechanisms and example of the metal oxide-coated FBG.

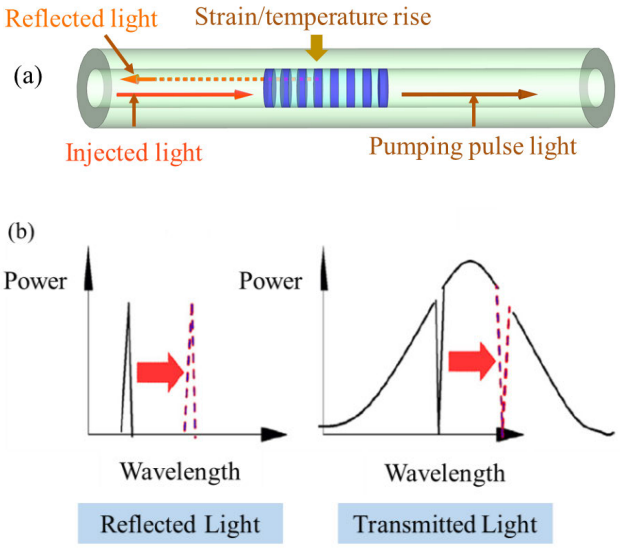

FIGURE 1. Sensing principle of fiber Bragg grating sensor. Adopted from [46]. (b) Expected output [46].

1) UNIFORM FIBER BRAGG GRATING

The first type of FBG is the uniform fiber Bragg grating (FBG). In a uniform FBG, the grating of the fiber maintains uniformity across the entire structure of the FBG [41]. The uniform FBG possesses a distinctive spectral characteristic: the ability to reflect a specific wavelength of light while transmitting others. This property has garnered the attention of researchers for use in sensing purposes. For instance, research conducted by Malakzadeh et al. [42] utilized this uniform FBG for temperature and strain sensing. Meanwhile, in RH sensing, the uniform FBG is also being employed to detect different RH levels using various sensitive coating materials to enhance the sensor's performance [43], [44], [45]. An illustration of a uniform FBG example is provided in Fig. 1 (a).

a: SENSING MECHANISM OF UNIFORM FIBER BRAGG GRATING

As the light is illuminated through the optical fiber, a tiny quantity of light is reflected at every periodic change. When the grating period of the fiber sensor is about half the wavelength of the input light, the reflected light signals combine coherently to produce a single large reflection at a specific wavelength. The grating will not influence the light traveling at wavelengths other than the Bragg wavelength which fulfils (1),

$$\lambda_B = 2n\Lambda \tag{1}$$

where λ_B is the Bragg wavelength, n is the effective reflective index of the grating inside the fiber core and Λ is the grating period [18]. In humidity sensing application, the change in RH can cause a change in the effective RI of the FBG, which in turn causes a shift in the Bragg wavelength. This shift can be measured and used to determine the RH [43].

b: METAL OXIDE COATED UNIFORM FIBER BRAGG GRATING

Research conducted by Nemeth Macambira et al. in 2019 [43] utilized graphene oxide (GO) as the coating material where they deposited GO on the FBG surface by dripping it onto the fiber surface. Subsequently, they injected a laser light with a central wavelength of 1046 nm and a power of 50 mW, inside the FBG for one hour. As a result of this process, a portion of the laser's energy was converted to heat, leading to an increase in FBG temperature. Consequently, the solubility of FBG decreased, and the GO was deposited on the FBG's surface. This deposition technique is known as optical deposition. The optical micrograph of FBG without and with GO coating is shown in Fig. 2.

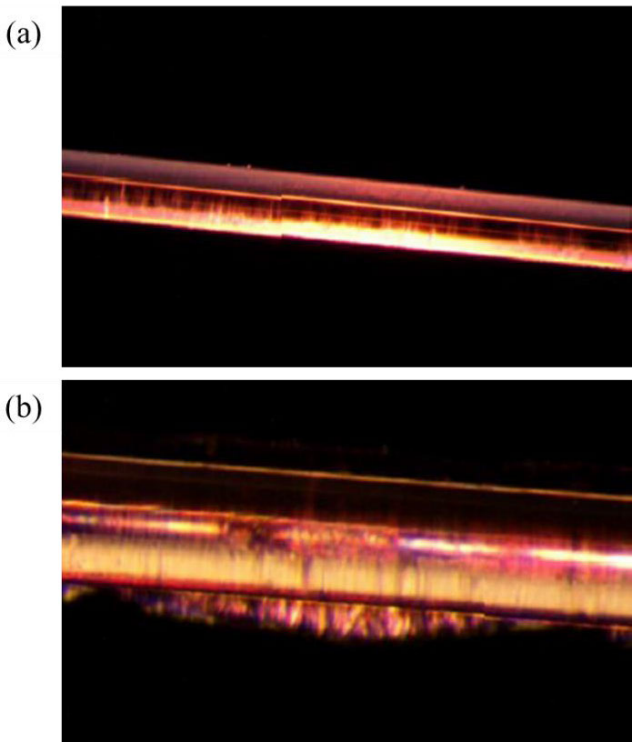

FIGURE 2. The optical micrograph of FBG (a) without GO (b) coated GO film [43].

In this work, relative humidity level was varied between 20% and 70%. The measurement of transmission spectrum was recorded by RH's interval of 10%. Fig. 3 displays the transmission spectra of the FBG coated with GO under different RH conditions. When the RH was below 20%, the fiber surface's refractive index experienced minimal alteration due to a limited presence of water molecules penetrating the GO film. As a result, the transmission spectrum of the FBG remained almost unchanged. On the other hand, when the RH exceeded 70%, the adsorption of water molecules by the GO films saturated. Consequently, as the RH continued to increase beyond this point, the RI of the fiber hardly changed, and the central wavelength of the transmission spectrum stabilized. From Fig. 3 (a), it is evident that the peak wavelength shifts to a higher wavelength as the RH increases. This study also revealed a good linear correlation between humidity and wavelength shift, with a sensitivity of 0.00253 nm/%RH and a linear coefficient of 0.9984.

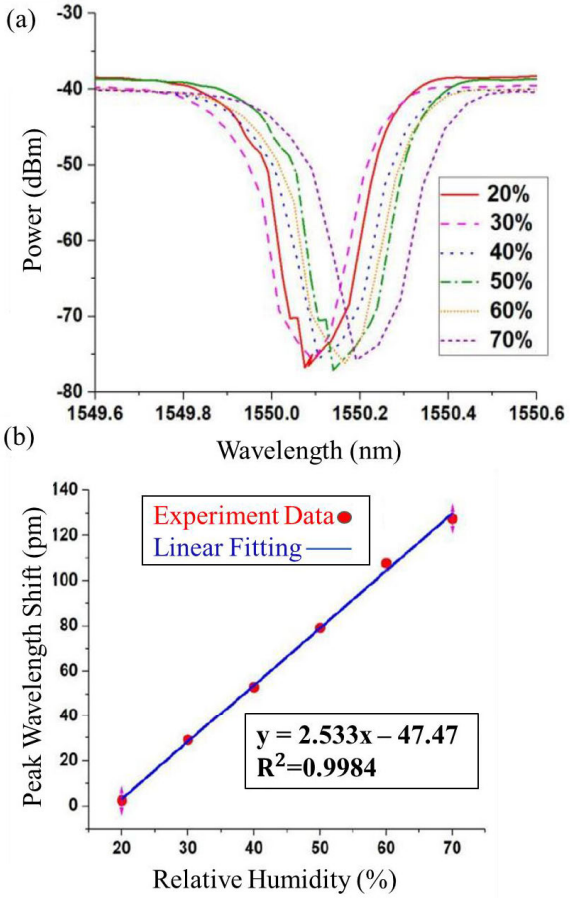

FIGURE 3. (a) Transmission spectra of GO-coated FBG at different relative humidity percent (b) The relationship between relative humidity and peak wavelength shift [43].

2) TILTED FIBER BRAGG GRATING

Tilted fiber Bragg grating (TFBG) is one of the optical fiber gratings where the grating plane is tilted at a particular angle with respect to fiber axis as illustrated in Fig. 4 [35], [36], [37]. The tilted angle within the grating plane and the fiber axis will result in the transmission spectrum producing many resonances and causing further complex mode to couple. The mode coupling in TFBG includes the core and mode coupling and the core and radiation coupling. The transmission characteristic of the TFBG gives a lot of information based on the fiber and grating structures, as the tilt and refractive index modulation play a pivotal role in determining the coupling efficiency and cladding mode resonance bandwidth [13].

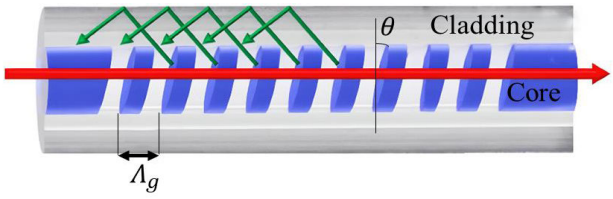

FIGURE 4. Tilted fiber Bragg grating [13].

a: SENSING MECHANISM OF TILTED FIBER BRAGG GRATING

Fig. 4 depicts a flat phase plane that is perpendicular to the guide shaft, which elucidates the mode fiber coupling between wave vectors. This coupling takes place along the fiber axis, leading to the creation of a uniform axial conduction mode. The resonant wavelength for the Bragg condition in a regular fiber grating can be denoted by (1), which can be written as (2).

$$\lambda_{Bragg} = n_{eff,core} n_{eff,core} \Lambda_g \tag{2}$$

The coupling between forward-propagating core modes and back-propagating core modes accounts for the Bragg resonance condition. As the grating plane is tilted with respect to the fiber axis, the grating period along the fiber axis can be mathematically represented by (3).

$$\Lambda_g = \frac{\Lambda_g}{cos\theta} \tag{3}$$

By substituting (3) to (2), the Bragg resonant wavelength is equals to,

$$\lambda_{Bragg} = (n_{eff}^{core} + n_{eff}^{core}) \frac{\Lambda_g}{cos\theta} \tag{4}$$

The tilted angle between the grating plane and the fiber axis gives rise to the coupling between a portion of the light that propagates forward in the core and the light that propagates backward in the cladding. The mathematical representation for the resonant wavelength of the cladding is as follows:

$$\lambda_{cladding,i} = (n_{eff}^{core} + n_{eff,i}^{cladding}) \frac{\Lambda}{cos\theta} \tag{5}$$

$n_{eff,i}^{cladding}$ is the refractive index of the i^{th} cladding mode. From (5), if the refractive index rises, the wavelength will also be increased or redshifted [13]. For humidity sensing applications, when the water is adsorbed by sensing material, the resonance wavelength of the cladding will be changing as

the refractive index of the sensing material is changed. From (5), the refractive index will change as the relative humidity rises, making the wavelength shift.

b: METAL OXIDE COATED TILTED FIBER BRAGG GRATING

This section focuses on the application of a metal oxide coating for tilted fiber Bragg grating (TFBG) in humidity sensors. Graphene oxide (GO), one of the metal oxides discovered between 2017 to 2021, was used as the sensing material due to its large surface-area-to-volume ratio and high absorption property across a broad range of wavelengths, thus making it suitable for use in optical fibers for UVA and biochemical sensing [38]. To coat the GO on the tilted fiber, a piezoelectric injection method was used, with the aim to provide a uniform coating and fast processing, making it ideal for humidity sensors. The TFBG used in the research work conducted by Chiu et al. was produced by inscribing single mode fiber (SMF) using phase mask technique, followed by spraying an aqueous solution of GO onto the optical fiber surface [13]. The grating plane had a tilted angle of 10 degrees, and the grating length was 5 mm.

To ensure secure adhesion of the GO on the fiber surface, the coated fiber was subjected to a piezoelectric injection process. This involved raising the coated fiber to 100°C, facilitating the evaporation of solvent and enhancing the bonding of GO. Following this, the fiber was placed in a humidity chamber maintained at a constant temperature of 27°C, with a relative humidity range spanning from 20% to 80% for humidity sensing purposes. The thickness of the GO coating was measured to be 1 μm using scanning electron microscopy (SEM), and an SEM image of the GO-coated optical fiber is shown in Fig. 5.

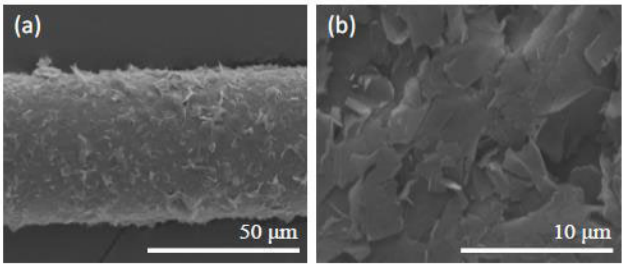

FIGURE 5. SEM image of GO coated optical fiber at 50 μm. (b) SEM image of GO coated optical fiber at 10 μm [13].

When GO coating on a tilted fiber Bragg grating (TFBG) was exposed to moisture, the water molecules were absorbed on the GO layer, causing the gap between the coating and optical fiber to change. Specifically, as the relative humidity increased, the gap between the two layers increased as well, which then altered the external refractive index of the TFBG.

Chiu et al. conducted a study on TFBG with different etching diameters and found that 20 μm diameter had the best sensitivity for humidity sensing [13]. Response and recovery times of the TFBG coated with GO and etched with 20 μm diameter were observed to be 12.25 min and 21.75 min, respectively, when the RH was changed from 20% to 80% RH.

From Fig. 6, the refractive index decreases when the humidity increases, shifting the wavelength from long to short wavelength. For example, when RH was 20%, the wavelength was measured at 1535.962 nm, and when RH was 80%, the wavelength was ascertained at 1535.367 nm. A total of 595 pm of wavelength shift was determined when RH was changed from 20% to 80%. This translated to sensitivity of 0.01 nm/%RH.

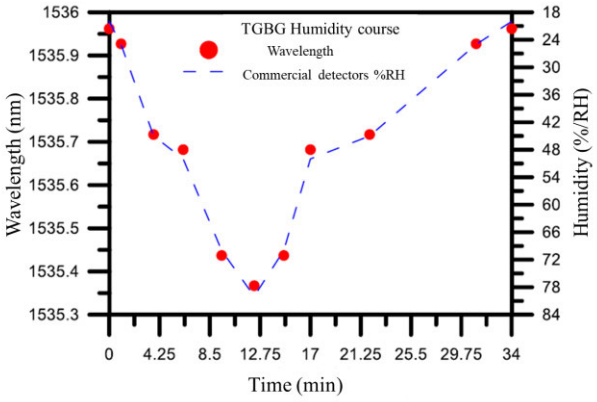

FIGURE 6. Response and recovery time of TFBG sensor for 20% to 80% RH [13].

Jiang et al. also used GO-coated TFBG for ultrafast humidity sensing application. The TFBG was fabricated using scanning phase-mask technique, with grating plane inclined at an approximate angle of 82°, and the grating length of 15 mm [38]. The GO was coated on the TFBG using the dip-coating technique, and multiple coating processes were performed to achieve the desired thickness. The coated fiber was immersed for 20 minutes and dried for 5 minutes for each coating process, resulting in a deposited GO layer with ∼54 nm thickness. The coated fiber was placed in a humidity chamber with RH % range from 30% to 80% RH. They deduced that as the RH increased, the GO film absorbed a higher amount of water molecules, increasing the refractive index and resulting in a redshift of the resonance wavelength. The sensitivity of GO-coated TFBG was measured to be 0.0185 nm/%RH, which was higher than the uncoated TFBG. The graphene sheets in metal oxide coated fiber sensor contained hydroxyl and epoxide groups. These groups maintained the relative interlayer distance of the crystallites and construct 2-D GO nanochannels. The constructed nanochannels enabled smooth movement for single-layer water molecules, and the rate of water molecule transported through the channels, formed by the interstitial spaces amid micro-sized crystallites, was approaching 1 ms^{-1}. This property promotes metal oxide coated fiber sensors effective for fast response properties in humidity sensing applications.

By comparing the two research works executed using GO as a coating material for TFBG, the research done by

Jiang et al. in 2019 showed higher sensitivity compared to Chiu et al. in 2017. The reason for sensitivity difference was mainly attributed by TFBG tilt angle. Jiang et al. employed a higher tilted angle at ∼82° with 15 mm grating length, resulting in the resonant wavelength of the cladding to have higher increment as the RH was increased. Even though Jiang et al. recorded higher sensitivity (0.0185 nm/%RH) compared to Chiu et al. (0.01 nm/%RH), it should be noted that their work were being carried out at different RH settings. As mentioned earlier, one of the most vital properties of the RH sensor is its response and recovery time. The response and recovery time recorded by Chiu et al. were 12.25 min and 21.75 min, respectively. On the other hand, Jiang et al. achieved 0.042 s and 0.115 s for response and recovery time, making it more acceptable for humidity sensing applications. The summary of these two research is demonstrated in Table 1.

3) TAPERED FIBER BRAGG GRATIN

Tapered fiber Bragg gratings (TFBGs) are another type of optical fiber gratings used for sensing applications. TFBGs consist of two transition regions where the fiber diameter slowly reduces and enlarges [47]. As light travels through the optical fiber, the energy inside the fiber core is confined within reflective boundaries. When incident broadband light passes through the fiber core and reaches the FBG, it is reflected only at the Bragg wavelength, λ_{Bragg}z [39].

a: SENSING MECHANISM OF TAPERED FIBER BRAGG GRATING

Referring to Fig. 7, Zhang et al. explained that the remaining energy is transmitted along the tapered region, known as the evanescent field [39]. TFBGs are more sensitive than standard optical fibers due to the mode confinement at the core and cladding interface. In a tapered FBG, the light is focused on the thin core until the mode guidance becomes weak and expands. The mode is then guided by the cladding/air interface, where the mode diameter is at its maximum and exposed to maximum confinement. The sensitivity of a TFBG depends on geometrical parameters such as taper length and diameter. The tapered region permits maximum interaction with the surroundings, making it vital for sensing applications.

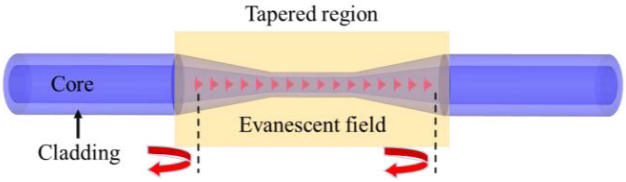

FIGURE 7. Tapered fiber Bragg grating. Adopted from [39].

The evanescent wave (EW) spectroscopy around the tapered region can be used to measure the environment's chemical composition since it has high sensitivity. The penetration depth d_p of the EW decay can be calculated by this equation,

$$d_p = \frac{\lambda}{2\pi \left(n_{eff}^2 - n_s^2\right)^{\frac{1}{2}}} \tag{6}$$

where λ is the wavelength of light in free space, n_{eff} is the effective RI of the mode guided by the optical fiber and n_s is the RI of the surrounding environment. The penetration depth (d_p) of the EW decays exponentially with the space between the waveguide and the surrounding environment, with a smaller penetration depth indicating a higher sensitivity [48]. Therefore, controlling the penetration depth is crucial in designing optical fiber sensors with high sensitivity for various sensing applications.

b: METAL OXIDE COATED TAPERED FIBER BRAGG GRATING FOR HUMIDITY SENSING

An example of metal oxide used for coating the tapered FBG for humidity sensing is zinc oxide (ZnO). ZnO has been broadly utilized for humidity sensing applications. This is because ZnO has a good photoelectric characteristic, surface absorption activity, and desirable structure, thus making it ideal for a broad scope of applications in environmental protection, photodetection, and sensing devices [49], [50]. Apart from that, ZnO's surface contains a lot of oxygen vacancies, which can help to increase active interaction between nanostructures and water molecules for improved humidity sensing performance [51], [52], [53]. Yu et al. in their research, stated that through physical adsorption, the O_2 was usually adsorbed on the ZnO's surface. Following this adsorption, the O_2 obtained negative electrons from ZnO to produce O_2^- on the surface of ZnO. The vacancy of oxygen defects on the surface of ZnO promotes dissociation of water molecules and facilitates the adsorption of oxygen. The higher number of surface oxygen vacancy defects will provide a higher opportunity for the water molecules to be absorbed on the surface of ZnO [49].

Aris et al. conducted research by coating tapered FBG with ZnO using the dip-coating method [54]. Before the coating process, the fiber was etched and the FBG diameter was measured at 84.74 μm. After undergoing the coating process, FESEM was used to observe the ZnO nanostructures on the tapered FBG and the image of grown ZnO is shown in Fig. 8.

Then, this coated tapered FBG is placed in a humidity chamber consisting of saturated salt solution for RH ranging from 55% to 80%. The tapered FBG was illuminated with amplified spontaneous emission (ASE) as a broadband light source. The uncoated and ZnO coated tapered FBG experienced wavelength shift of 35.3 pm and 61.5 pm, respectively, as displayed in Fig. 9.

The coated ZnO achieved higher sensitivity (0.0025 nm/% RH) than the uncoated fiber (0.0014 m/%RH). This is because the absorption of the water molecule by ZnO will generate more strain and trigger a higher shifting of the Bragg wavelength, resulting the sensor to be more responsive towards humidity. In conclusion, the use of ZnO as sensing

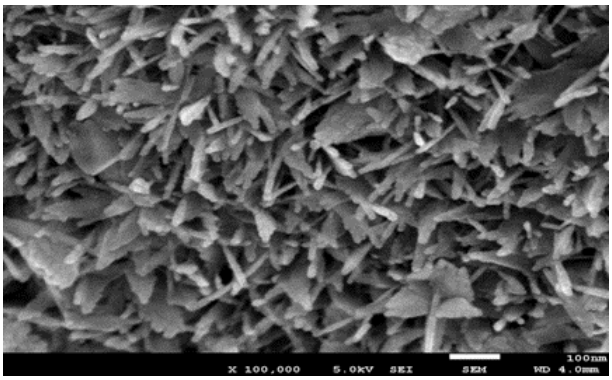

FIGURE 8. FESEM image of ZnO nanostructures grown on tapered FBG [54].

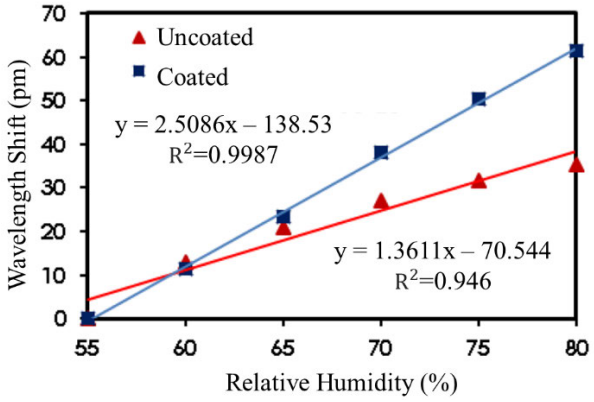

FIGURE 9. Wavelength shift of uncoated and ZnO coated tapered FBG against RH % [54].

material succeeded in increasing the sensor's sensitivity by 85%.

4) LONG PERIOD GRATING

Long period grating (LPG) contains a few centimeters long optical fiber with periodic perturbation in its refractive index or geometry. The period is usually in the range of 100 to 1000 μm [55], [56], [57], [58]. The schematic of long period grating used for sensor application is illustrated in Fig. 10.

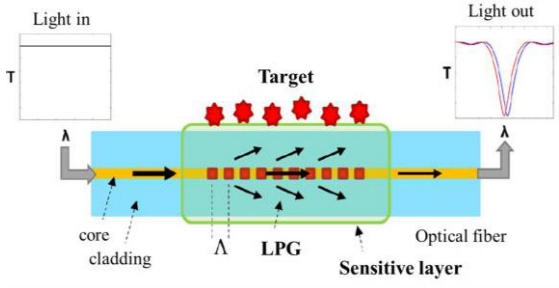

FIGURE 10. Schematic diagram of long period grating in sensing application [59].

The LPG schematic diagram consists of an LPG transducer inscribed onto an optical fiber. This fiber includes a responsive layer that enhances its receptiveness to changes in the refractive index of the surrounding medium, thereby enabling the detection of the intended analyte.

a: SENSING MECHANISM OF LONG PERIOD GRATING

The grating encourages the coupling between the light from the fundamental core mode to forward propagating cladding modes. This results in discrete attenuation bands that are visible in the fiber transmission spectrum, as shown in Fig. 10. These bands are located at wavelength $\lambda_{res,i}$, which fulfills the phase-matching requirement, given by equation (7) below:

$$\lambda_{res,i} = \left(n_{eff,co} - n_{eff,cl}^{(i)}\right) \cdot \Lambda \tag{7}$$

where $n_{eff,co}$ is the effective refractive index of the core mode, $nw_{eff,cl}^{(i)}$ is the refractive index of the i^{th} cladding mode and Λ is the period grating [55]. The attenuation bands have the transmission value at the resonance wavelength can be determined by:

$$T_i = cos^2\left(k_i \cdot L\right) \tag{8}$$

where L is the grating length and k_i is the coupling coefficient for the i^{th} cladding mode [59], [60].

The vital characteristic of the LPG is that the resonance wavelength and the amplitude of attenuation bands are influenced by external environment which the outer layer of the fiber is subjected to. This is in contrast with the traditional emphasizing on the core and cladding refractive index for phase-matching conditions [55], [61]. The phase-matching condition is satisfied if the external RI is smaller than the RI of the cladding. Then, the effective refractive index of the cladding will be increased and at the same time, retaining the RI of the core, the resonance wavelength will shift from high to low wavelength [62]. If the external RI surpasses the effective RI of the cladding, the phase-matching condition is no longer met. As such, internal reflection is no longer maintained at the interface between the cladding and the surrounding medium. As a result, the guided modes within the cladding behave like radiation modes. In this case, wavelength shift does not take place, but the intensity of the resonance loss band will change. The change of intensity is determined by the quantity of light reflections occurring at the interface between the cladding and the surrounding medium.

b: METAL OXIDE COATED LONG PERIOD GRATING FOR HUMIDITY SENSING

The example of metal oxide used in coating LPG for humidity sensing application is graphene oxide (GO). GO is a two-dimensional nanomaterial consisting of sp^2 and sp^3 hybridized carbon atoms accompanied by a bunch of oxygen-rich functional groups. The oxygen-rich functional group enables GO to be used in sensing applications where the GO is coated on the fiber surface using dip-coating technique

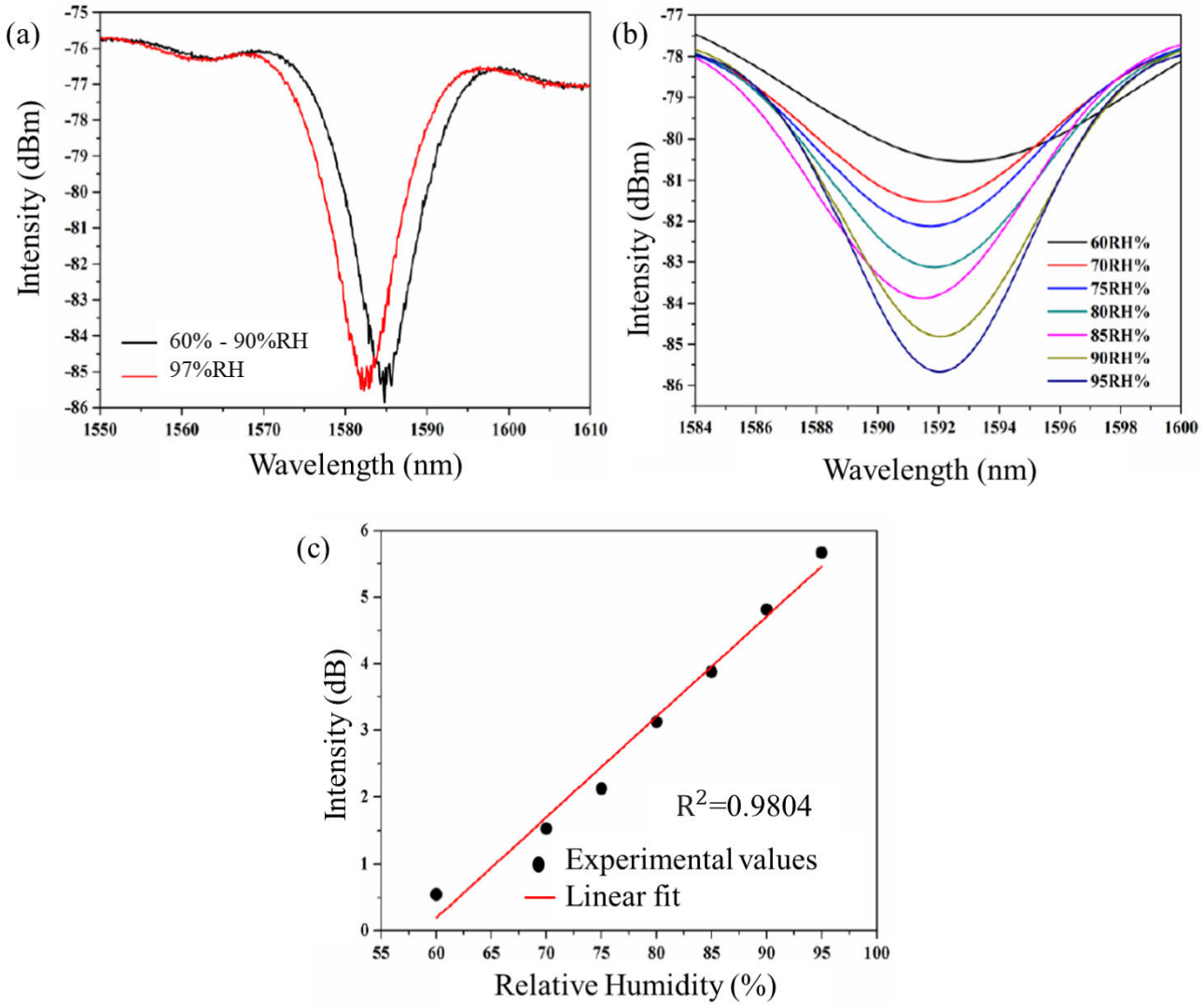

FIGURE 11. (a) Uncoated LPG response on humidity changes. (b) Transmission spectra of GO coated LPG. (c) Intensity variations of the resonance band centered at 1592 nm at different RH% [62].

[62]. To ensure the stability of coating and the immobilization of GO flakes, the silica fiber surface is functionalized using 3-(trimethoxysilyl)propyl methacrylate before conducting the coating process. The estimated coating thickness in this study was approximately 1.5 μm. This research tested the GO coated LPG by placing the fiber in a humidity chamber. The relative humidity was studied within the range of 60% to 95% RH. To investigate the sensor performance on relative humidity, one end of GO coated LPG was attached to the broadband light source through single-mode fiber (SMF), while the other side was connected to the optical spectrum analyzer (OSA) to note the transmission spectra.

The experiment started by monitoring the performance of the uncoated LPG for humidity sensing. The result showed that there was no change on the transmission spectrum when the uncoated LPG was exposed to RH lower than 96%. However, as the RH reached 97%, slight changes in the intensity and wavelength of the resonance band occurred, as shown in Fig. 11 (a). It was deduced that for RH higher than 97%, the water droplet could be possibly deposited on the uncoated fiber surface. This occurrence caused measurement error due to the strain exerted on the LPG because of these deposited droplets. The research was continued by observing GO coated LPG by changing the RH% from 20% to 95%. As shown in Fig. 11 (b), the transmission spectra exhibited resonance band centred at wavelength of 1592 nm. Since the wavelength revealed a small shift for RH lower than 60%, the experiment focus was narrowed, concentrating on range 60% to 95% RH. Fig. 11(c) shows that when the humidity percentage was increased, the intensity of the resonance band also increased as well, for 60% to 95% RH. The change of the center wavelength and intensity of the resonance band

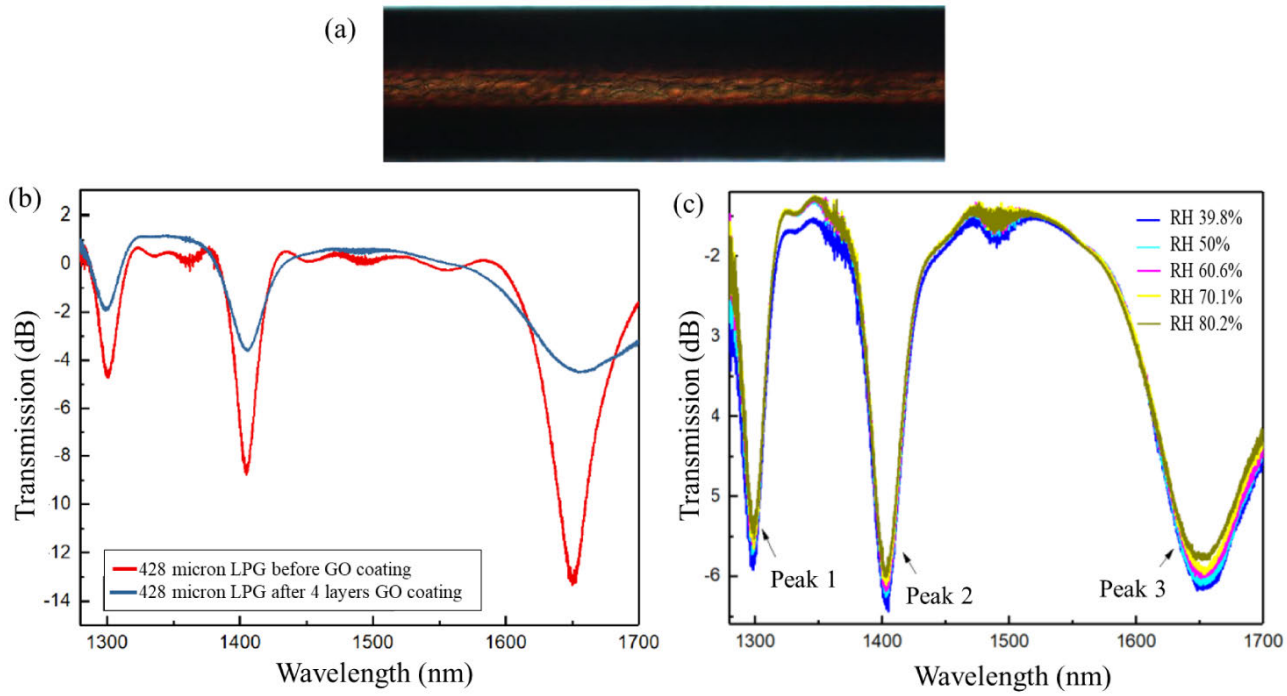

FIGURE 12. (a) The microscope image of GO-coated LPG and (b) transmission spectrum of 4 layers GO-coated LPG. (c) The transmission spectrum of the 4-layer GO at different RH level [63].

was attributed to the difference in optical properties. These differences were related to changes in the RI and coupling coefficient of GO material when exposed to water molecules. The sensitivity of GO coated LPG in this study was revealed at 0.15 dB/%RH over the range of 60% to 95%RH at 25 °C.

In 2020, research executed by Sahoo et al., also used GO as the coating material for LPG with the same deposition method [63]. The fabrication of the LPG involved the utilization of the point-by-point technique, where a collimated UV beam exposure was used to achieve the periodic refractive index modulation of the fiber. The designed LPGs had a period of 428 μm and a length of 20 mm. In comparison to previous research, this study covered a slightly lower relative humidity (RH) range, specifically from 40% to 80% RH. In contrast, the study by Dissanayake et al. examined a broader RH range, ranging from 60% RH to 95% RH. In this work, they studied on 2- and 4- layers of GO. The microscope image of GO-coated LPG and transmission spectrum of 4 layers GO-coated LPG is shown in Fig. 12 (a) and (b).

The graph demonstrates a noticeable reduction in the attenuation bands of the three coupled cladding modes after GO was coated on LPG. This reduction was more pronounced at for the peak observed at 1650 nm. The intensity of this peak decreased from 15 dB to 4 dB. This change could be attributed to the presence of the additional GO film layer on the surface of the LPG, which alters the cladding mode coupling coefficient.

For RH sensing performance, this study varied the RH from 40% to 80%RH with a step of 10% at a constant temperature, 25 °C. The results revealed that the 4-layers GO-coated significantly more responsive to RH changes compared to 2-layers of GO. The transmission spectrum of the 4-layer GO is shown in Fig. 12 (c). In the graph, all the peaks exhibited variation as the RH is varied, indicating that the 4-layer GO was more sensitive when exposed to different RH. The sensitivity of the 4-layer was calculated to be 0.0084%/RH, whereas the 2-layer GO-coated sensor recorded a sensitivity of 0.000025%/RH. The sensitivity of 4-layers GO was increased by 33 times. This study proved that apart from the metal oxide coating, the thickness of coating also played a crucial role for humidity sensing at different RH.

One recent work in 2021 using GO coated S-type LPG was conducted by Tsai et al. [64]. The coating technique employed in this study was piezoelectric inkjet, and the S-type LPG was fabricated through a lithography process using SU-8 305 negative photoresist and an etched single-mode fiber (SMF). Fig. 13 (a) and (b) show the fabricated optical microscope image and scan emission microscope image of the sensor, respectively. The SMF was subjected to wet etching, resulting in three different diameters: 37 μm, 42 μm, and 60 μm. After analyzing the resonance wavelength shift and the transmission loss of the resonance dip for these three diameters, they concluded that 37 μm was the optimal fiber diameter. When subjected to RH levels spanning from 20% to 80% RH, the 37 μm diameter recorded the highest sensitivity at 0.17773 dB/% RH with strong linearity of 0.9661. In contrast, the widest diameter (60 μm) sensor recorded sensitivity of 0.0351 dB/% RH, with a lower

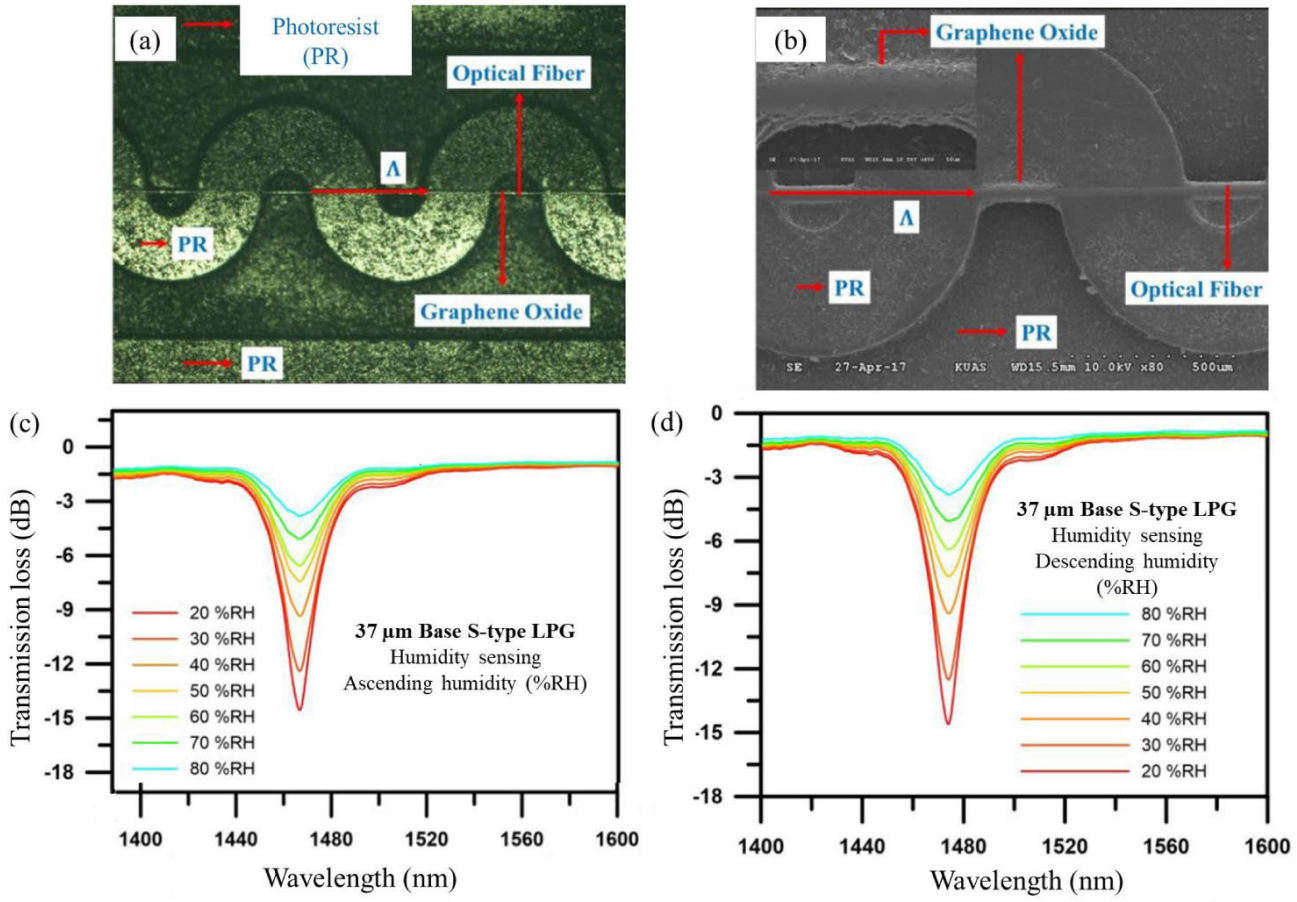

FIGURE 13. Transmission spectrum of S-type long period grating at (a) ascending RH and (b) descending RH [64].

linearity of 0.9574. The transmission spectrum of the sensor with a diameter of 37 μm is shown in Fig. 13 (c).

From the study, it was proven that the sensitivity of the RH sensors was inversely proportional to the fiber diameter. The results obtained for the three mentioned diameters denoted a consistent trend: as humidity increased from 20% RH to 80% RH, the RI of GO decreased accordingly. The presence of more water molecules caused a decrease in the refractive index of the graphene oxide, leading to a reduction in the resonant dip of the coated LPG. Conversely, when relative humidity decreased, the transmission loss of the resonant dip escalated. This is due to the liberation of water molecules from the GO film, causing the effective refractive index of the coating materials to rise.

Furthermore, this study also investigated the effect of descending humidity to the sensor by introducing dry air. This approach was undertaken to reduce the resonance attenuation dip of the sensor. The transmission spectrum of descending RH for the first cycle is shown in Fig. 13 (d). The experiment was repeated three times to study the repeatability of the RH sensor.

Through curve fitting analysis, as the humidity decreased from 80% to 20% RH, the sensitivity of the base S-type LPG sensor documented values of 0.1797, 0.1819, and 0.1856 dB/% RH for the first, second, and third cycles correspondingly. Moreover, the linear fit of the response exhibited correlation coefficients of 96.97%, 95.86%, and 95.62% for the corresponding cycles. This study recorded the highest sensitivity during the third cycle of dehumidification. In comparison to the three previously discussed studies that used the same material, GO to coat LPG, this study achieved the highest sensitivity at 0.1856 dB/% RH with correlation coefficients of 95.62%. The sensitivity demonstrated in study is slightly higher than the study reported by Dissanayake et al. (2018), where a sensitivity of 0.15 dB/%R was recorded. Additionally, the sensitivity obtained in this study was 18 times higher than the result reported by Sahoo et al. which was 0.0084%/RH [62], [63]. The summaries of the three research studies that utilized long period grating as a sensing mechanism are presented in Table 1.

5) MICRO-NANO STRUCTURED FIBER BRAGG GRATINGS

One of the drawbacks of commonly used FBGs fabricated by SMF is their limited sensitivity in detecting the evanescent wave, primarily attributed to the constraints of the thick

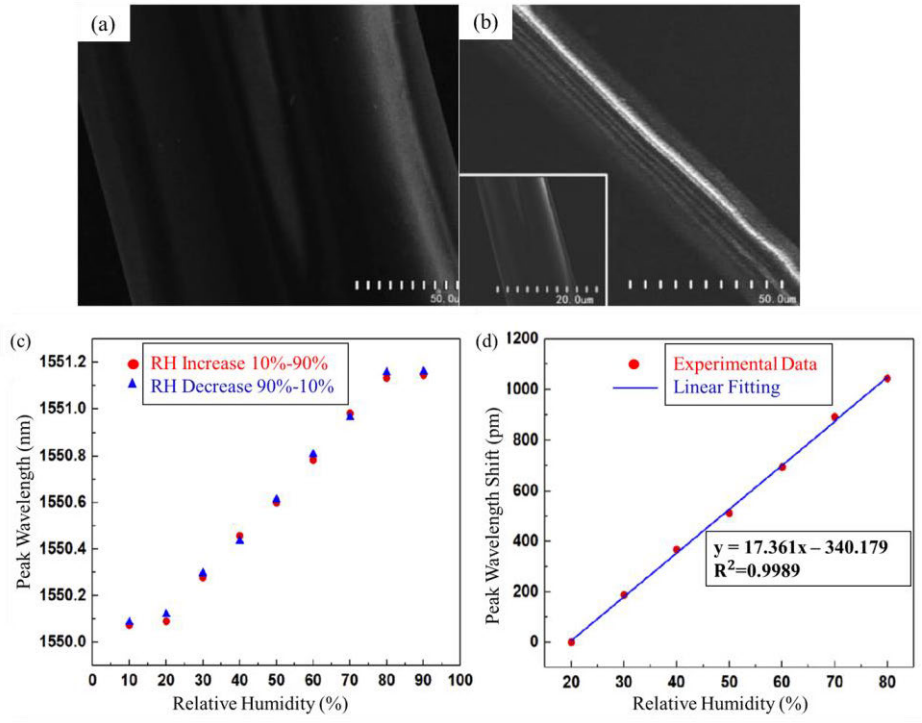

FIGURE 14. (a) Scanning electron microscopic images of (a) fiber Bragg grating (b) micro/nano fiber Bragg grating and sensor's characteristics (c) variation of the peak wavelength (d) peak wavelength shift at different relative humidity level [65].

cladding layer [65]. To overcome this limitation and enhance the interaction between the light field and the environmental medium, micro/nano fiber Bragg gratings (MNFBGs) are utilized. MNFBGs are a type of fiber Bragg grating fabricated in a micro/nanofiber using femtosecond pulse irradiation, nanoimprinting technique, and chemical corrosion method [65], [66]. Compared to common FBGs, MNFBGs are smaller in size, making them favorable for applications where size is important, such as in medical instrument applications [67], [68]. Besides, MNFBGs are also being used in RH monitoring. Research conducted by Li et al. [65] utilized this FBG structure coated with GO to monitor different concentrations of RH ranging from 20% to 80%RH.

The MNFBGs was fabricated using a chemical corrosion technique and the creation of the consistent grating was achieved through the utilization of a phase mask made from zero-order fused silica, featuring a period of 1059.39 nm. For MNFBG fabrication, hydrofluoric acid (HF) was used for corrosion process. The corrosion time was increased from 15 minutes to 30 minutes, resulting in diameter grids ranging from 105 μm to 12 μm. In this study, the grid area employed was 12 μm (with 30 minutes corrosion time), as smaller grid area was known to enhance sensitivity. The reflected spectrum of the fiber was shifted from 1552.826 nm (FBG) to 1550.065 nm (MNFBG). The images of FBG and MNFBG were also observed using SEM and are shown in Fig. 14 (a) and (b). From the SEM images, the diameter of the FBG noticeably decreased from 125 μm to 12 μm. The reduction in diameter allowed stronger evanescent field to penetrate the surrounding medium, increasing the interaction with the medium and enhancing the sensor's sensitivity.

The study was continued by coating the MNFGB with GO using optical deposition. The reflected spectrum of GO-coated MNFBG was compared with the uncoated fiber and it was found that the power was increased approximately 1 dB. This enhancement was attributed to the role of GO, which served as the cladding and effectively confined the optical signal within the core. The size of GO flakes obtained was about 2 μm with thickness of 2.5 μm. These measurements aligned with the findings of previous study carried out by Jiang et al. [38]. He mentioned that the capability of the GO film to absorb water molecules was influenced by its thickness. If the GO film was extremely thin, for instance 5 layers (approximately 6 nm), or exceedingly thick, reaching 20 μm, its capability to absorb water would be diminished. A thin GO film absorbed only a small amount of water molecules would restrict the humidity detection range. On the other hand, excessive thickness in the GO film would change the RI of the outer layer (near the air) with varying water absorption. Meanwhile, the RI of the inner layer (near the MNFBGs surface) remained relatively constant due to the restricted permeation of water molecules [38].

The RH sensing performance using GO-coated MNFBGs was observed in RH range 20% to 80%RH with increment of 10%. It was found that, at RH levels below 20%, the central wavelength of the reflected spectrum experienced minimal

TABLE 1. Sensing performance of metal oxide coated fiber bragg grating.

Sensing Technique	Sensing Material	Coating Technique	Sensitivity	Response Time	Recovery Time	Reference
Uniform FBG	Graphene Oxide, GO	Optical deposition	0.00253 nm/%RH (20% to 70%RH)	N/A	N/A	[43]
Tilted FBG	Graphene Oxide, GO	Piezoelectric inject	0.01 nm/%RH (20% to 80% RH)	12.25 min	21.75 min	[13]
		Dip coating	0.0185 nm/%RH (30% to 80%RH)	0.042 s	0.115 s	[38]
Tapered FBG	Zinc Oxide, ZnO	Dip coating	0.00251 nm/%RH (55% to 80% RH)	N/A	N/A	[54]
Long period grating	Graphene Oxide, GO	Dip coating	0.15 dB/%RH (60% to 95% RH)	N/A	N/A	[62]
		Dip coating	0.0084%/RH (40% to 80%RH)	N/A	N/A	[63]
		Piezoelectric inkjet	0.1856 dB/% RH) (20% to 80%RH)	N/A	N/A	[64]
Micro-nano FBG	Graphene Oxide, GO	Optical deposition	0.017361 nm/%RH (20% to 80%RH)	3.2 s	8.3 s	[65]

change. This was due to the insufficient penetration of water molecules through the GO film, resulting in little variation in the effective RI. Conversely, when the RH exceeded 80%, the central wavelength became more stable owing to the saturable of water molecule absorption by the GO film. Despite further increment in RH, the effective RI remained unchanged. The changes of peak wavelength and the corresponding wavelength shift are plotted against varying RH, as shown in Fig 14 (a) and (b). This study recorded the sensitivity of 17.361 pm/RH% with response and recovery time of 3.2 s and 8.3 s, respectively. The finding from this work as well as those from the use of other metal oxides in coating four types of FBG are summarized in Table 1.

From Table 1, only two types of metal oxides have been employed as coating materials for fiber Bragg grating optical fiber humidity sensors: GO and ZnO. Among these, GO is the more commonly used material, with seven out of eight studies utilizing it to enhance the performance of the FBG sensors. In terms of sensitivity, a study conducted by Jiang et al. [38] reported that GO achieved the highest sensitivity at 0.0185 nm/%RH, covering a wide range of relative humidity (RH) from 30% to 80% RH. In comparison, the study by Aris et al. [54] recorded a sensitivity of 0.00251 nm/%RH using ZnO but with a narrower RH range (55% to 80% RH). Regarding response and recovery times of the humidity sensor, GO exhibited a rapid response with a recovery time of 0.042 seconds and 0.115 seconds, respectively. However, it's worth noting that the studies utilizing ZnO as the coating material did not provide information on this particular parameter.

B. INTERFEROMETER

Interferometer-based optical fiber sensors offer a highly responsive foundation for sensing applications. The interferometer's performance is influenced by the interference between higher order modes with the fundamental modes, resulting in variations in resonance wavelength. The phase shift in the optical spectrum relies upon the optical path length of the interference mode, which can be expressed as the following (9).

$$\phi = \frac{2\pi}{\lambda}\left(\delta n_{eff}\right) L \tag{9}$$

In (9), λ is the wavelength, L is the sensing length, δn_{eff} is the refractive index difference between the higher order and the cladding modes [69]. There are two main components in the interferometer sensor, which are the sensing arm and reference arm [69]. The guided light will be split into a separate path; the light travels through the sensing arm will exposed to the sensing medium, meanwhile the light propagating in the reference arm is isolated from the sensing medium. The constructive and destructive interference will be generated depending on the two arms' in phase and out of phase conditions. Two types of interferometers will be discussed in this review, namely Mach-Zehnder and Michelson interferometers.

1) MACH-ZEHNDER INTERFEROMETER

Mach-Zehnder interferometer (MZI) has been broadly utilized in sensing applications such as humidity and temperature sensing applications due to its flexible structure and compactness [69], [70], [71], [72]. To construct an MZI, two taper regions are necessary as optical components. These tapered regions enable efficient transfer of a significant portion of light energy from the fundamental mode to the cladding modes. As the guided light propagates into the first tapered region, the energy distribution of the fundamental mode faces difficulty to maintain the local fundamental mode within the tapering section due to its short diameter. Consequently, the mode leaks through the cladding region, resulting in the conversion of the fundamental mode's energy loss into higher order cladding modes. This phenomenon is referred to as the core-cladding transition. At the steep slope of the tapered region, a significant number of modes are excited and coupled to the guided light, transitioning into higher order modes, as depicted in Fig. 15. These higher order modes subsequently couple back to the fundamental mode at the second tapered section, generating spectrum interference.

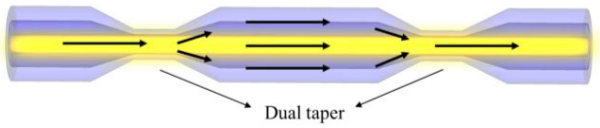

FIGURE 15. Schematic diagram of dual taper used to realize MZI. Adopted from [69].

a: SENSING MECHANISM OF MACH-ZEHNDER INTERFEROMETERS

The Mach-Zehnder interferometer operates based on the measurement of phase shift occurring between two beams [73]. The interference is generated due to the difference in optical path lengths between the sensing and reference arms, despite these arms being physically equal in length. During the sensing operation, the sensing arm interacts with the environment while the reference arm remains isolated. Changes in the surrounding parameters introduce phase shifts, consequently leading to patterns of constructive or destructive interference [69]. Commonly, MZI is based on multimode interference and the schematic diagram of MZI is shown in Fig. 16.

The output intensity of the interference pattern can be calculated using the following equation,

$$I = I_1 + I_2 + 2\sqrt{I_1 I_2 cos\phi} \tag{10}$$

where I_1 and I_2 are the intensity of the propagating light and ϕ is the phase difference. The phase difference can be obtained by using the following formula,

$$\phi = \frac{2\pi}{\lambda}\left(\Delta n_{eff}\right) L \tag{11}$$

where Δn_{eff} is the effective RI between the core and cladding of the fiber and L is the sensing length.

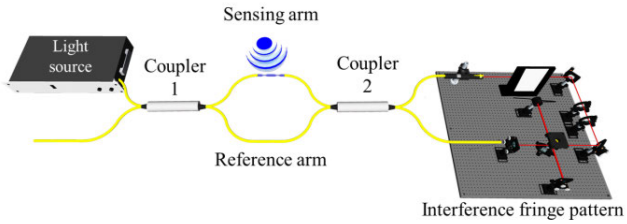

FIGURE 16. Schematic diagram of dual taper used to realize MZI. Adopted from [69].

b: METAL OXIDE COATED MACH-ZEHNDER INTERFEROMETERS

A few types of metal oxide have been discovered and are used for coating Mach-Zehnder interferometers for humidity sensing application. In a study conducted by Lokman et al., ZnO was chosen as the sensing material for coating an Inline Mach-Zehnder interferometer (IMZI) [14]. The fabricated dumbbell-shaped IMZI used in this research is shown in Fig. 17. The two fabricated bulges had diameter of 198 and 196 μm, respectively, with the tapered waist diameter in between them measured at 95 μm. The two bulges were separated at by 1000 μm gap, and the humidity sensor employing the IMZI relied on the signal interference between core and cladding modes within this dumbbell configuration. These bulges functioned as a beam splitter and beam combiner. In the first bulge, which served as a beam splitter, the cladding modes were excited and passed through the fiber cladding and the surrounding coating layer, while some light continued to propagate inside the core. In the second bulge, which functioned as a beam combiner, part of the cladding modes was recoupled into the core of the SMF. Hence, IMZI was created from the optical phase difference between the core and higher-order cladding modes.

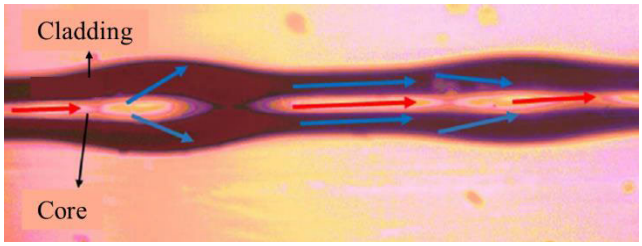

FIGURE 17. Microscope image of fabricated dumbbell-shaped IMZI [14].

The nanowires ZnO coating IMZI structure was achieved by dip-coating the IMZI structure into the ZnO solution obtained using the sol-gel method. The dip-coating process was repeated five times, and followed by drying the IMZI for each dip-coat at 60 °C. The purpose of drying was to facilitate evaporation the solvent and get rid of the organic residuals. The experiment was conducted by placing the coated IMZI inside the humidity chamber with a saturated salt solution to vary the RH from 35 to 60% RH. As the ASE laser source was ejected through the IMZI sensor, the

sensor probe generated a sinusoidal-like reflected spectrum. The emergence of sinusoidal-like spectrum was attributed to the difference of optical path between the cladding and core modes, resulting an interference pattern in the IMZI. Variation in the RH percentage induced changes in the RI of the surrounding medium. The variance in RI modified the output of the transmission spectrum. As the RH percentage increased, the resonant wavelength of the probe was red-shifted. For example, the resonant wavelength of one of the peaks shifted from 1553.715 to 1554.205 nm as RH percentage increased. The red shifting was due to the rise of surrounding RI, hence reducing the phase difference between the core and cladding modes.

To observe the effectiveness of ZnO coating on the IMZI, the experiment was conducted for both uncoated and coated ZnO. The ZnO-coated IMZI showed remarkable improvement in sensitivity, elevating it from 0.0001 nm/%RH to 0.0205 nm/%RH. The increased sensitivity was a result from the interaction of ZnO and surrounding high humidity. Under such conditions water molecules were confined between the nanowires mesh due to electrostatic force. Instead of air, the nanowire meshes trapped the water molecules, causing a linear change in the RI of the ZnO coating with the increment of RH. This phenomenon occurred due to the fact that RI of water (1.333) is greater than the RI of the air (1.001). As the RI of the surrounding changed, the path length difference between the core and cladding modes within the IMZI also changed accordingly. This resulted in shifting the interference spectrum to a longer wavelength. This explanation aligned with the result obtained from the experiment carried out by Lokman et al. [14]. The observed response time of this sensor was less than 5 s which was considered a fast response time.

In another research, Liu et al. used a different type of metal oxide: graphene oxide (GO) [74]. In their study, they utilized the core-offset MZI by splicing three sections of SMFs with a small lateral offset, as shown in Fig. 18 (a). The GO was deposited on the core-offset MZI by using dip-coating technique. As shown in Fig. 18 (a), when light was ejected towards the first core-offset MZI via SMF1, the misalignment of core diameters caused the excitation of higher order modes. During the forward transmission of the light, a part of the light entered the core of SMF2, referred as core modes. Simultaneously, the remaining portion was coupled into SMF2's cladding, denoted as cladding modes. Because of the phase difference between the core and cladding modes, interference occurred at the second core-offset structure, followed by their re-coupling with SMF3. Consequently, both intensity and wavelength of the resonant dips of the MZI experienced variations.

This research was conducted with RH% ranging from 30% to 60%. As indicated in Fig 18 (b), with increasing RH%, the extinction ratio of the transmission spectra diminishes from around 22 dB to approximately 16 dB at the resonant dip located at 1545.7 nm. A portion of the light escaped as it traversed the cladding and encountered interference between the cladding and the GO composite film. This was due to the cladding's refractive index being lower than that of the GO composite film. Conversely, the RI of the GO composite film decreased as the RH was raised, owing to its increased water absorption. This caused a reduction in the RI difference between the cladding and the GO composite film. Hence, there would be a decrease in light leakage, leading to a reduction in extinction ratio of the transmission spectrum.

The sensor's sensitivity was observed by plotting the fitting line of the resonant dips at the wavelength of ∼1545.7 nm across various RH levels, as illustrated in Fig. 18 (c) above. From the fitting line, the sensitivity of the sensor was estimated at 0.104 dB/%RH with a linear coefficient of 99.61%. As shown in Fig. 18 (b), the transmission dip A shifted to shorter wavelength when the RH was reduced from 60% to 30%. The fitting line of the transmission dip A with different levels of RH is depicted in Fig. 18 (c).

The sensor's sensitivity was observed by plotting the fitting line of the resonant dips at the wavelength of ∼1545.7 nm across various RH levels, as illustrated in Fig. 18 (c) above. From the fitting line, the sensitivity of the sensor was estimated at 0.104 dB/%RH with a linear coefficient of 99.61%. As shown in Fig. 18 (b), the transmission dip A shifted to shorter wavelength when the RH was reduced from 60% to 30%. The fitting line of the transmission dip A with different levels of RH is depicted in Fig. 18 (d). From the fitting line, the sensitivity of the sensor was determined to be 0.0272 nm/%RH. The sensitivity of uncoated core-offset MZI was also investigated, and the sensitivity was observed at 0.0032 nm/%RH, which was lower compared to the GO-coated core-offset MZI. This research showed that coated metal oxide's on the core-offset MZI successfully increased its sensitivity as the uncoated core-offset MZI sensitivity was only one-tenth of the sensitivity of coated MZI.

Furthermore, research conducted by Fan et al. also involved GO as the coating material for the MZI humidity sensor. In their study, the MZI was constructed through the fusion splicing of a segment of few-mode fiber (FMF) between two segments of no-core fiber (NCF), which functioned as couplers [75]. The schematic diagram of few-mode MZI with NCF-FMF-NCF structure is illustrated in Fig. 19 (a).

Referring to the structure in Fig. 19 (a), when the light enters from SMF1 to NCF1, part of the light will be coupled into the cladding of FMF. This coupling leads to the excitation of cladding modes caused by the mismatch between the core diameters. At the same time, the other part of the light will propagate inside the core of FMF, exciting the fundamental and high-order modes. Then, both lights in core and cladding modes continue to travel inside FMF at different propagation constants and interfere at the FMF-NCF2-SMF2 region, with most of the lights coupled into the SMF2.

In this research, the GO sheet was coated on the FMF to increase the moisture absorption capacity for humidity sensing. This study was conducted with RH% ranged from

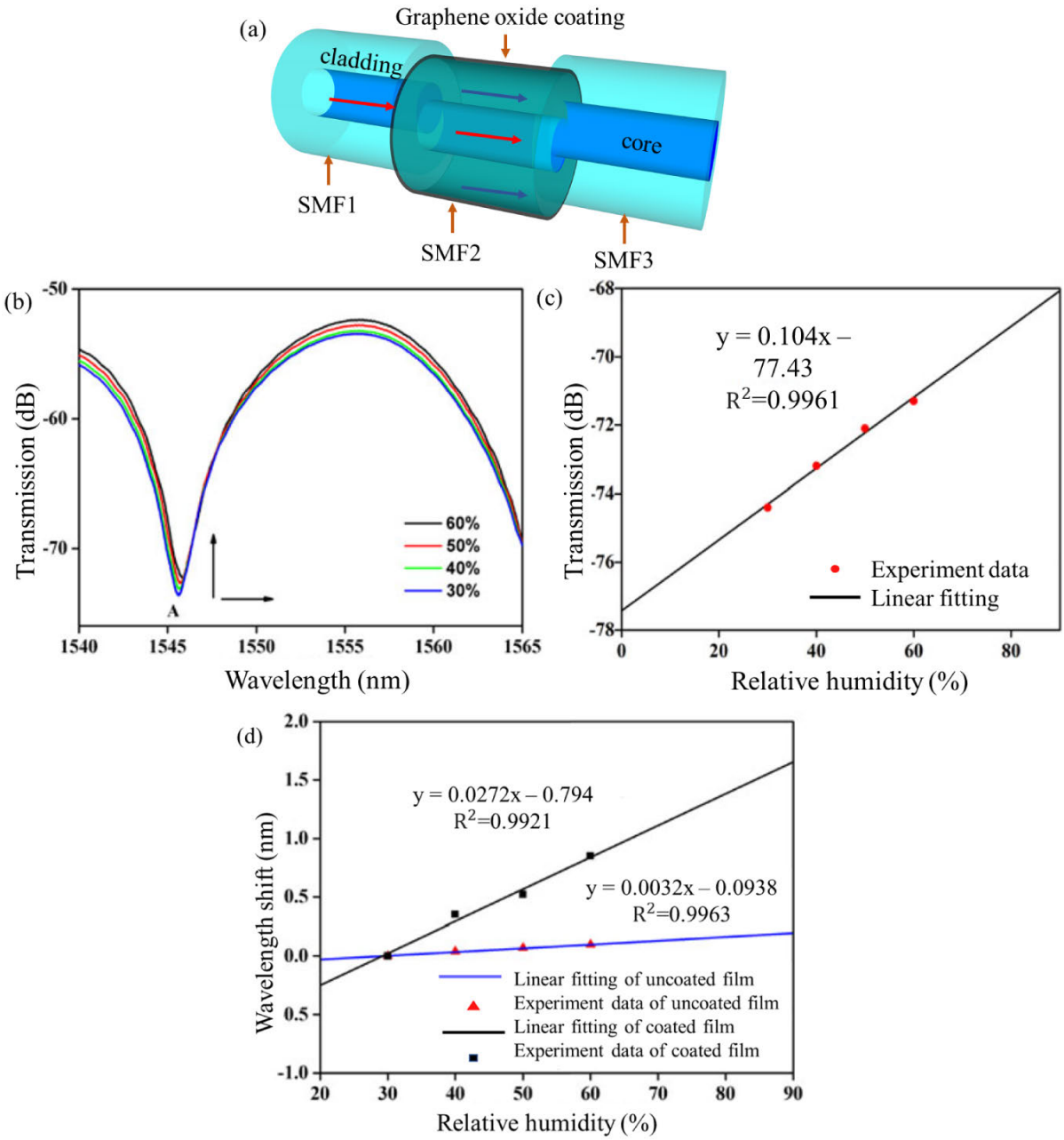

FIGURE 18. (a) Schematic diagram of core-offset Mach-Zehnder interferometer. Adopted from [74]. (b) Transmission spectrum of the core-offset MZI coated GO film under different RH from 30% to 60% RH. (c) Fitting line of the resonant dips at the wavelength of ~1545.7 nm with variation of RH%. (d) Fitting line of the measured wavelength shift of the transmission dip A with variation of RH and fitting line of uncoated MZI with RH changing from 30% to 60% [74].

30-95%, with the constant temperature at 25 °C. The transmission spectrum of the sensor is shown in Fig. 19 (b).

From Fig. 19 (b), it is evident that as the RH increases, the wavelengths are shifted to the left. A clear linear correlation is detectable within the RH 30-50% and 55-95%. The sensor recorded higher sensitivity 0.191 nm/%RH at lower RH and lower sensitivity 0.061 nm/%RH at RH 55-95%. This can be explained that GO sheet in lower RH had a larger gap, facilitating the absorption of water molecules, causing the significant changes in n_{eff} of the cladding mode, resulting in larger wavelength shifts. Meanwhile, at higher RH, only a small amount of water molecules could be absorbed due to the gradually saturated GO sheet. It caused only a slight change in the n_{eff} and smaller wavelength shift. The relationship between the resonance dip near 1564 nm and RH% is plotted and is shown in Fig. 19 (c). From the fitting line at 30-50%RH and 55-95%RH, the sensor's sensitivity is obtained as the values mentioned before.

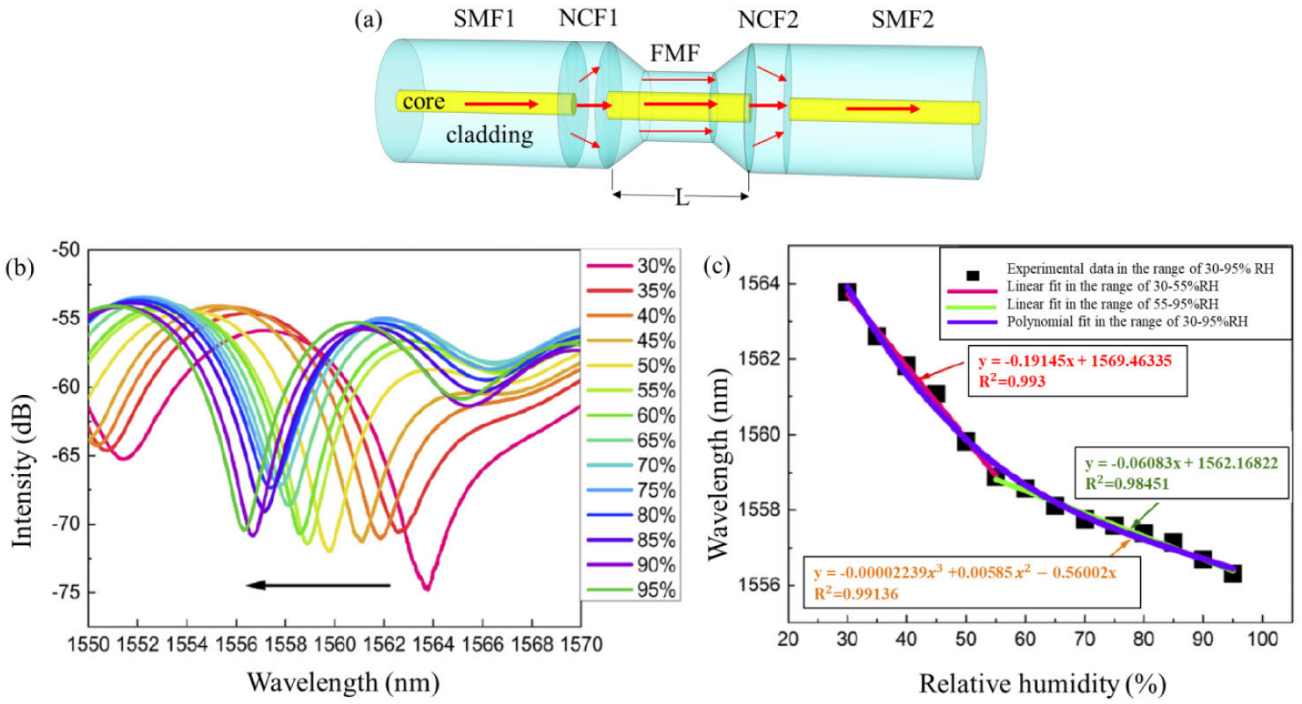

FIGURE 19. (a) Schematic diagram of few-mode Mach-Zehnder interferometer. Adopted from [75]. (b) Transmission spectra of the sensor with RH from 30-95%. (c) Relationship between the wavelength of the resonant dip∼1564 nm and RH [75].

Next, research accomplished by Wang et al. [76] also employed GO to coat the RH sensor. In this study, a core-offset MZI was used to detect RH ranging from 35.3% to 95.8%RH. The schematic representation of the core-offset MZI sensor used in this study is depicted in Fig. 20 (a). The nonaligned structure illustrated in the figure was assembled using a fiber fusion splicer, and GO was coated within the core-offset region to act as the sensing element. This study used the same sensing mechanism as research conducted by Liu et al. [74] wherein the difference in optical path lengths for two light beams transmitted along the core and the cladding led to their recombination in the final SMF segment, resulting in interference. Typically, the RI of the cladding was influenced by changes in the surrounding RI, while the RI of the core remained unchanged. However, in this specific structure, due to variations in the effective RI resulting from alterations in the external RI, this configuration could be employed to quantify shifts in external parameters.

Prior to the relative humidity (RH) sensing exploration, a coating of graphene oxide (GO) was applied to the core-offset region using a drop casting technique, with 2-3 layers applied and subsequently dried within a blast drying oven to create a GO-film. The light emitted from the light source was directed into the first SMF, passing through the coated area. The difference in effective RI caused a shift in the interference spectrum. The transmission spectrum of the sensor at various RH levels is depicted in Fig. 20 (b). From the transmission spectrum, it is evident that the graph experienced a red shift with a displacement of 4 nm, while the depth of interference reaches 19.84 dB. Additionally, this study evaluated the response time, which was measured at 7 s. The long response time was due to relation time of sensitive material. In the case of GO at micron scale, the relaxation time was 6.4 s. The sensitivity of this sensor was calculated from the wavelength shift when the RH changes is equal to 0.05 nm/%RH with linearity of 88%. The linearity of this sensor was considered low due to the uneven thickness of the GO layers, as noted by the authors.

Another study also harnessed the potential of GO as the sensing material. In 2022, Fu et al. utilized a sensor comprising a concise segment of tapered dual side-hole fiber (DSHF), positioned between two SMFs. The illustration of this configuration along with the cross section and microscope image of the cone region are shown in Fig. 21 (a), (b) and (c) [77]. This investigation embraced the same sensing mechanism, where the light propagated inside the cladding (higher order mode) interfered with the fundamental mode that propagated inside the center of DSCF at the last SMF region. The resulting interference was observed due to the varying optical path lengths of the light. The DSCF was tapered using the oxyhydrogen flame heating technique and the GO was coated to the tapered-DSHF using the optical deposition. The utilization of GO as a coating material facilitated the absorption of water molecules. These water molecules were subsequently adhered to the GO surface or permeated the layers of the GO film. As a result, this process elevated the carrier density

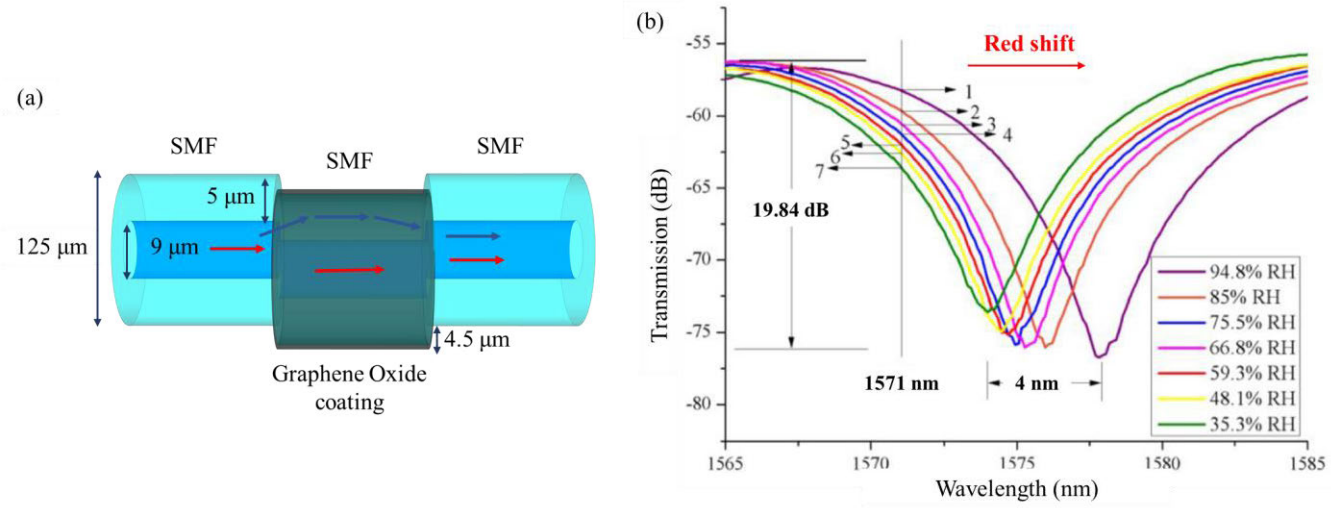

FIGURE 20. (a) Schematic illustration of core-offset Mach-Zehnder interferometer. Adopted from [76]. (b) Transmission spectrum of the relative humidity sensor at different RH level [76].

on the GO surface, leading to a decrease in the RI of GO. Thus, the effective RI of the mode decreased, and the distinct responses from the two modes contributed to the shift in the interference spectrum.

Firstly, the uncoated tapered-DSHF was examined under varying RH conditions, ranging from 35.2%RH to 66.3%RH. Subsequently, the performance of coated tapered-DSHF was observed. The sensitivity of uncoated tapered-DSHF was recorded as 0.016 nm/%RH, with a linear fitting degree at 99.3%. In contrast, the coated tapered-DSHF exhibited a sensitivity of 0.142 nm/%RH. Notably, the sensor's sensitivity increased by 7.9 times with the application of the GO coating. Then, the study was continued by varying the tapered-DSHF diameter at 9 μm, 15 μm and 23 μm. Among these, the 9 μm diameter exhibited the optimal performance with a sensitivity of 0.142 nm/%RH. The transmission spectrum of 9 μm with different RH levels, along with the graphical representation of the relationship between resonant wavelength and RH are shown in Fig 21 (d) and (e). These findings affirmed that the sensor's sensitivity increased by using smaller diameter of tapered fiber. However, it cannot be excessively small as this could lead to higher losses. This study also recorded the response and recovery time of the optimal sensor used were 0.23 s and 2.19 s, respectively.

The latest research involving the utilization of a metal oxide-coated MZI fiber sensor, which was conducted by Ding et al. in 2023. In this study, a balloon-like fiber interferometer was employed to detect varying levels of relative humidity (RH), ranging from 35% to 90% RH [78]. The configuration of the balloon-like sensing head is outlined in Fig. 22 (a). The fabrication of the balloon-like sensor involved bending a SMF and subsequently coating it with a layer of GO using a dip-coating technique. To understand the morphology and thickness of the coating, SEM is used for analysis. The SEM image of the GO-coated fiber is shown in Fig. 22 (b). From Fig. 22 (b), since the cladding diameter equal to 125 μm and the deposited SMF is about 125.5 μm, the sensing material was calculated to be 250 nm. Furthermore, a uniform distribution of GO nanomaterials can be observed in Fig. 22 (c).

This study identified the optimal sensitive length within the sensing region at bent diameter of 8 mm sensing region and determined the ideal thickness for coating material. The investigation continued by varying the sensitive length across 10 mm, 15 mm and 20 mm increments. Across all these three lengths, the sensitivity remained higher at low RH levels (less than 50%) compared to the sensor's performance at higher RH levels (more than 50%). This sensitivity disparity arose from the fact that at lower RH levels, the GO nanomaterial coating was dry and have a wider gap, resulting in more water molecules to enter the material. Thus, it caused greater change in effective RI, hence observing a larger wavelength shift. In contrast, as the RH levels increased, the adsorption of water molecules by GO materials gradually approached a state of saturation. As a result, the effective RI only have slight change causing a small wavelength shift. Among the three lengths, 20 mm exhibited highest sensitivity at 0.449 nm/RH when the RH level was varied. The transmission spectrum of 20 mm sensitive length with a red shifted graph is shown in Fig. 22 (d).

The high sensitivity observed at longer sensitive length suggested that the sensor's sensitivity correlated with the increment of sensing length. This outcome could be attributed to the fact that a longer sensitive length allowed greater coverage of the sensing region by GO nanomaterial. As mentioned earlier, this study also explored the optimal thickness of the GO coating by introducing two additional thickness levels, employing different ratios of deionized water to GO. The thickness 250 nm, which was previously employed was

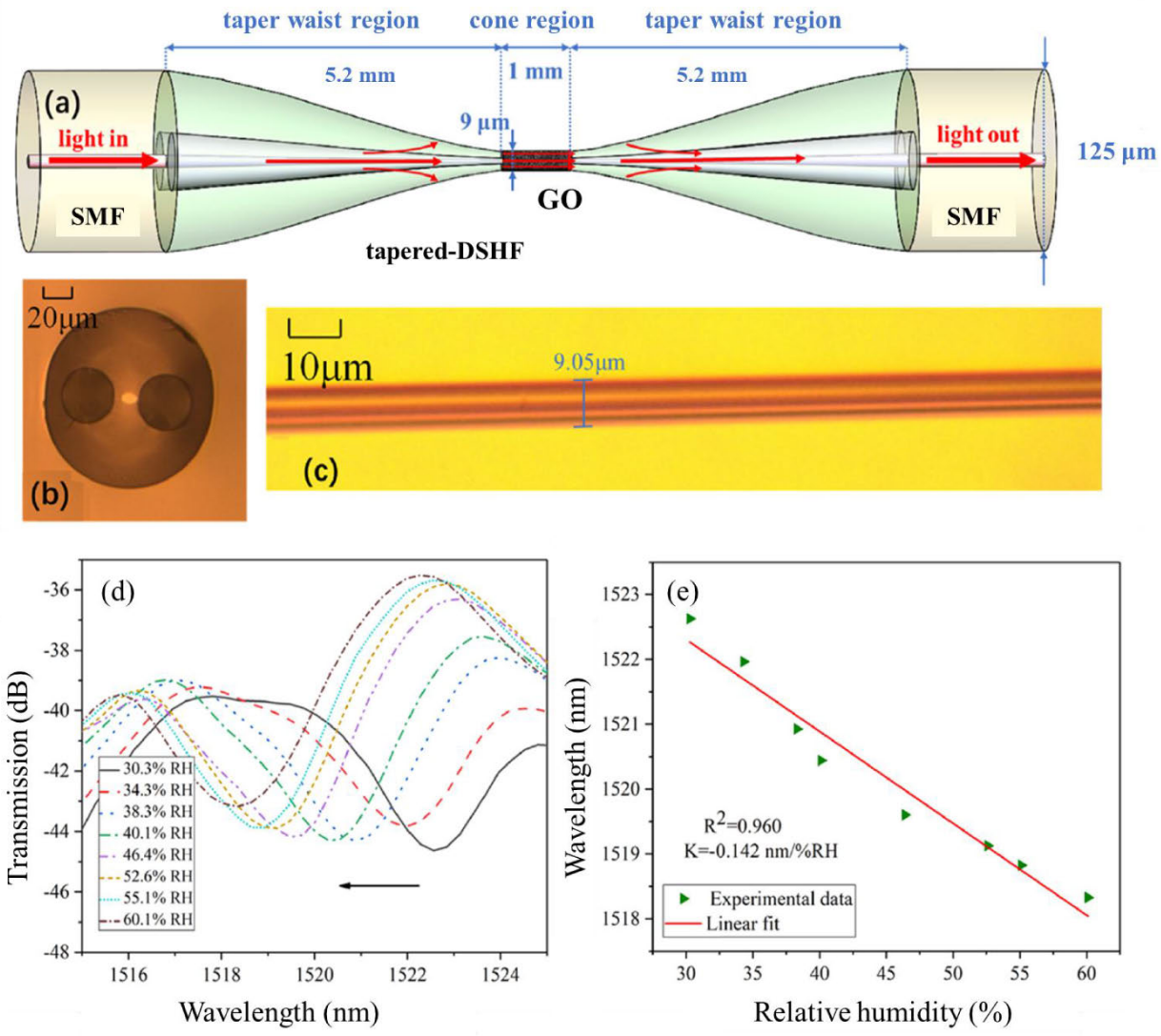

FIGURE 21. (a) Schematic illustration of tapered dual side hole fiber (DSHF). (b) The cross section of the tapered-DSHF. (c) The microscope image of tapered-DSHF. (d) Transmission spectrum of GO-coated tapered DSHF at different relative humidity level. (e) The relationship between the resonance wavelength and relative humidity [77].

prepared with a mixing ratio of 1:4. The other thickness had the mixing ratios of 1:5 (100 nm) and 1:3 (350 nm). Both the 1:5 and 1:3 mixing ratios recorded lower sensitivity with lower wavelength shift when the RI was varied. This sensor demonstrated highest performance with 20 mm sensitive length and a 250 nm GO thickness, yielding a sensitivity of 0.449 nm/RH. This study recorded response and recovery time of the sensor at 4.8 s and 7.8 s, respectively.

In this section, a summary of six research works was provided, highlighting the utilization of metal oxides as sensing material in Mach-Zehnder interferometer. Two types metal oxides were studied, namely ZnO and GO. Among these research studies, it was noteworthy that the investigation conducted by Lokman et al., which employing ZnO, recorded the lowest sensitivity at 0.0205 nm/%RH in comparison to other studies that utilized GO as the coating material. Notably, the sensitivity of the humidity sensor appeared to be significantly enhanced when GO was employed as the sensing material. This is due to the unique properties of GO that have a high number of oxygen-containing groups such as carboxyl, hydroxyl and carbonyl that are distributed in a random manner on the basal plane and edge plane, contributed to a higher amount of water molecules can be absorbed from the surrounding [74]. Meanwhile, when considering studies that employed the same coating material, GO, the research carried out by Ding et al. demonstrated the highest sensitivity, reaching 0.449 nm/RH. This particular study employed the MZI sensing mechanism, incorporating a balloon-like sensor configuration to detect various levels of relative humidity.

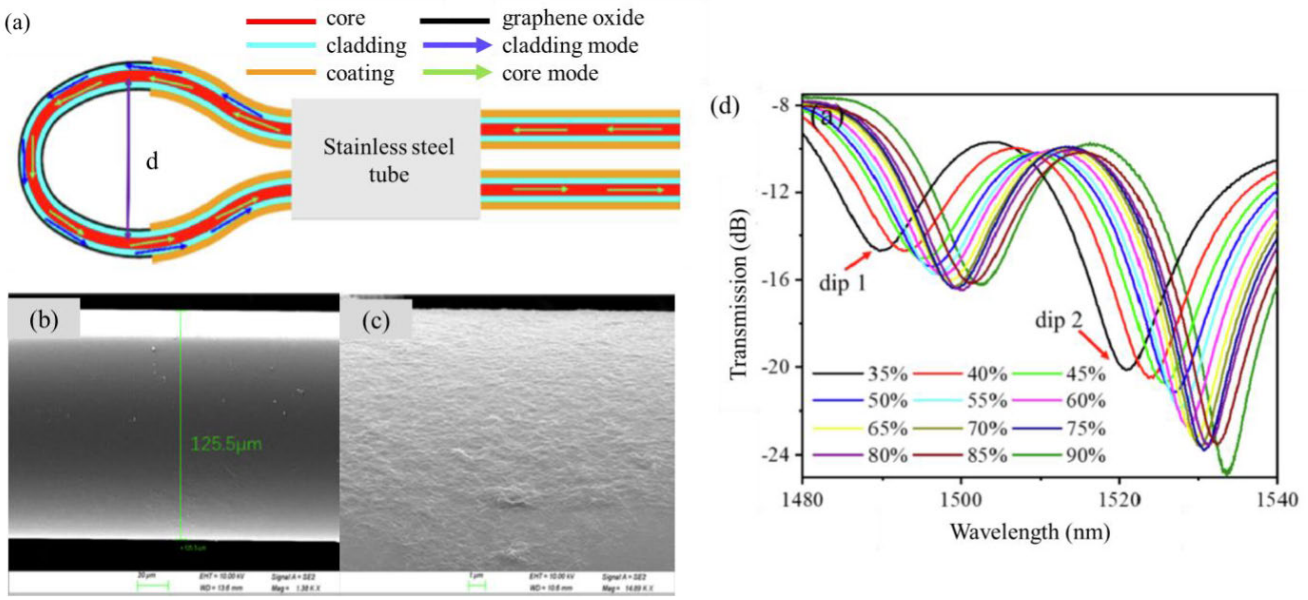

FIGURE 22. (a) Schematic diagram of balloon-like sensor. (b) SEM image of the fiber with graphene oxide coating. (c) The SEM of GO-coated on the fiber surface. (d) The transmission spectrum of 20 mm sensitive length of balloon-like sensor [78].

2) MICHELSON INTERFEROMETER

The second type of interferometer that has been widely used for sensing applications is the Michelson interferometer. Michelson interferometer can be constructed by linking two separate fiber pieces to the output ports of a fiber coupler and connecting 100% reflecting mirrors or Bragg grating at the opposite terminations of these fibers. This interferometer works much similarly to MZI, but the crucial difference between these two types of interferometers is that the light that propagates in its two arms is obliged to interfere at the same coupler where it split [79], [80], [81], [82]. The schematic diagram of the Michelson interferometer is shown in Fig. 23 (a). Agrawal also mentioned in his journal article that the interference that occurred at the same coupler made Michelson interferometer acting as a nonlinear mirror, which was similar to Sagnac interferometer. Nonetheless, a crucial differentiation is the optical fields involved in the interference in Michelson interferometer do not share an identical physical path [79]. The construction of the Michelson interferometer can be realized through either two-core fiber or by implementing beam splitters directly within the fiber structure. The Michelson interferometer made by two-core fiber will be discussed in detail in this discussion.

a: SENSING MECHANISM OF MICHELSON INTERFEROMETERS

Michelson interferometers operates similarly to MZI, relying on the phase shift measurement between two beams. However, in the Michelson interferometer, interference occurs at the same coupler. Chu et al. used a side polished twin-core fiber Michelson interferometer (SPTCFMI) to sense relative humidity [83]. The SPTCFMI is shown in Fig. 23 (b). Two cores, each with a diameter of 8.9 μm, were symmetrically positioned within the cladding, which measured 123 μm in diameter. The refractive index of the core was 1.448, and there was a RI difference of 0.0042 between the core and cladding.

Fig. 23 (c) illustrates the experimental setup using supercontinuum laser as the light source, an OSA, a fiber circulator and an SPTCFMI coated with metal oxide films. One end of the SPTCF was spliced to the SMF pigtail of the fiber circulator, while the other end was cleaved to achieve a 4% reflection at the interface between silica and air. The fusion and tapering process between the SMF and TCF was carried out with the aim to achieve a splitting ratio of approximately 50:50 in the two cores. This was essential to ensure a significant fringe visibility on the interference spectrum. The tapering process was terminated when the two cores possessed roughly equal energy, which could be observed through a beam view analyzer. Subsequently, the light was coupled into the TCF via the tapered region, and the reflected beam from the TCF's end would recombined along the same tapered section to establish the MZI. To determine the optical path difference (OPD), the fiber was subjected to bending, and the interference at the output of the circulator was observed.

The optical path difference between the interferometer's two arms without side polished surface is equal to an integer multiple of the wavelength. This is shown in (12) below,

$$2\left(n_1 L_1 - n_2 L_2\right) = m\lambda_m \tag{12}$$

where n_1 and n_2 are the effective RI of the two core modes and L_1 and L_2 are the length of the cores, m is an integer and λ_m is the wavelength of the interference peak. When the RI of the surroundings in the side-polished area undergoes alteration, the effective RI of the core mode region within

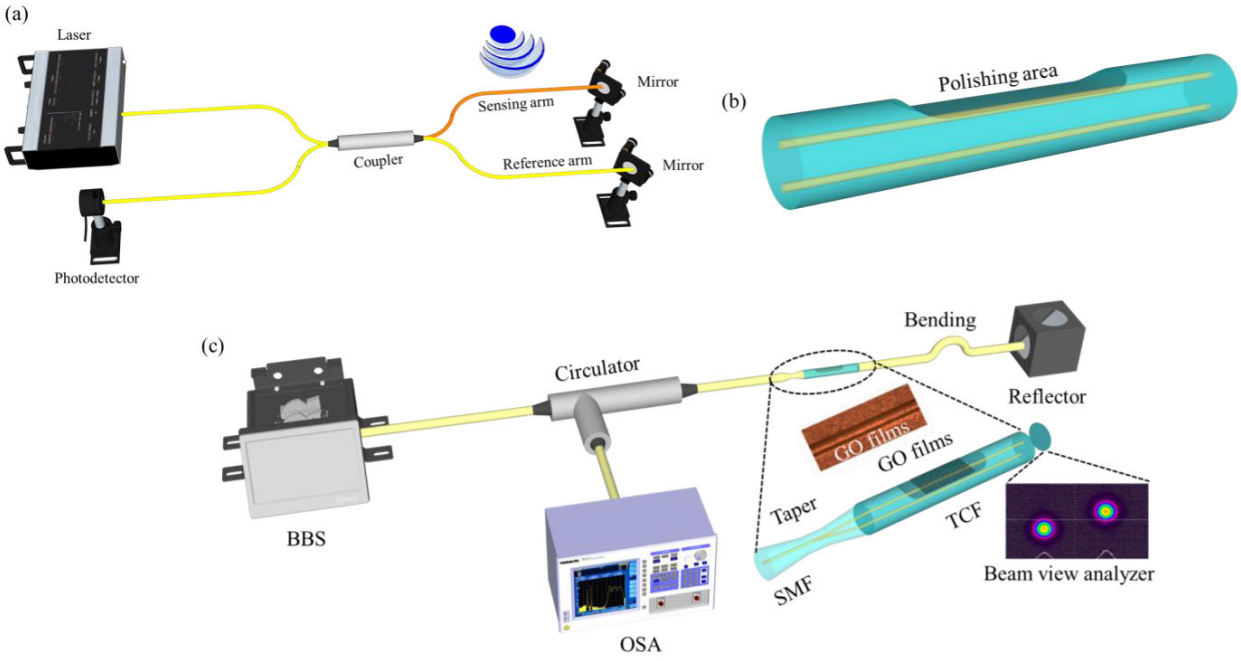

FIGURE 23. (a) Schematic diagram of Michelson interferometer. (b) Side polished twin-core fiber Michelson interferometer. (c) Humidity sensor set-up based on SPTCFMI coated with GO [51]. Adopted from [83].

the side-polished section likewise adjusts. This leads to a modification in the RI disparity between the two cores (Δn). The new optical path difference of the side-polished core mode is shown in (13), where l is the side-polished length.

$$2\left(n_1L_1 - n_2L_2\right) + 2\Delta n \cdot l = m(\lambda_m + \Delta\lambda) \tag{13}$$

Thus, the wavelength shift of the interference peak can be written as (14).

$$\Delta\lambda = \Delta n \cdot l \cdot \lambda_m / \left(n_1L_1 - n_2L_2\right) \tag{14}$$

b: METAL OXIDE COATED MICHELSON INTERFEROMETERS

Chu et al. experimented Michelson interferometers coated with graphene oxide films for humidity sensing [83]. The GO film was coated on a side-polished twin-core fiber Michelson interferometer using a multiple-drop-casting technique to ensure a smaller coated area and homogeneous thick GO film. To observe the effect of metal oxide coating on humidity sensing performance, the experiment was firstly conducted using uncoated SPTCF with the polished depth (d), 0 μm. The interference peak result showed only 0.13 nm peak shift in RH range from 40% to 75% RH, as shown in Fig. 24 (a). The small wavelength shifting of the peak indicated the change of RH in the surrounding side-polished region had weak influence on the polished core mode. On the other hand, Fig. 24 (b) depicts significant blueshift on the transmission spectrum with the increment of RH.

The application of a GO coating led to a rise in interferometer loss by approximately 1.5 dB due to the higher refractive index (RI) of graphene oxide. This resulted in an increased release of energy from the polished core. The sensitivity of the coated SPTCFMI was also higher than

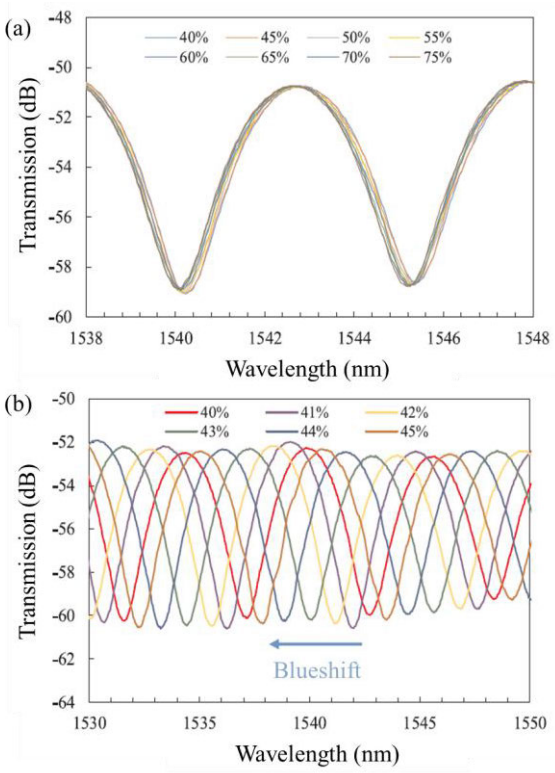

FIGURE 24. Transmission spectra of the SPTCFMI with different RH at d = 0 μm (a) uncoated (b) coated GO film [83].

uncoated fiber, where the sensitivities were ~1.191 nm/%RH and ~0.003 nm/%RH, respectively. The higher peak shift

TABLE 2. Sensing performance of metal oxide coated interferometers.

Sensing Technique	Sensing Structure Design	Sensing Material	Coating Technique	Sensitivity	Response Time	Recovery Time	Reference
Mach–Zehnder interferometer (MZI)	Inline	Zinc Oxide, ZnO	Dip coating	0.0205 nm/%RH (35% to 60% RH)	<5s	N/A	[14]
	Core-offset fiber	Graphene Oxide, GO	Dip coating	0.104 nm/%RH (30% to 60% RH)	N/A	N/A	[74]
	Few-mode fiber		Natural deposition	0.191 nm/RH% (30% to 55% RH) 0.061 nm/%RH (55% to 95% RH)	N/A	N/A	[75]
	Core-offset fiber		Drop casting	0.05 nm/RH% (35.3% to 95.8% RH)	7 s	N/A	[76]
	Tapered dual side-hole fiber		Optical deposition	0.142 nm/RH% (35.3% to 95.8% RH)	0.23 s	2.19 s	[77]
	Balloon-like fiber		Dip coating	0.449 nm/RH (35% to 90% RH)	4.8 s	7.8 s	[78]
Michelson interferometer	Side-polished twin-core fiber	Graphene Oxide, GO	Multiple-drop-casting	~2.72 nm/RH% (40% to 75% RH)	3.6 s	6.4 s	[83]

and the sensitivity of GO coated SPTCFMI were higher because the increasing of RH helped greater absorption of water molecules by the GO film. The absorption led to direct swelling of the GO layer and subsequently influenced the peak shift and sensitivity. Consequently, the expansion of the GO film could potentially contribute to the alteration of the effective RI of the GO film. In other word, graphene is prone to absorb polar molecules because of its ultrahigh carrier activity, in which the water molecules will act as electron acceptors.

When the water molecules were attached to the surface of the GO film, there would be a rise in the density of charge carriers (holes) within the GO. This resulted in the Fermi level of the GO to increase beyond the Dirac point and blocking interband transitions and elevating the graphene's chemical potential. Hence, the difference of refractive RI of the GO film was formed. As the amount of water being absorbed increased, the effective RI of the side polish core would reduce. Thus, the increase in RH influenced the resonant wavelength in the transmission spectra, shifting it to lower wavelengths. The research was further explored by varying the side-polished depth. It was observed that the sensitivity was increased to ~2.728 nm/%RH. This elevation in sensitivity was attributed to the enhanced evanescent field of the polished core, which interacted more significantly with the GO films. The response and recovery time of GO coated SPTCFMI were 3.6 s and 6.4 s, respectively and these timing were considered very fast. The findings from this research with earlier discussed research works that used metal oxide as sensing material are shown in Table 2.

From Table 2, two types of metal oxides have been identified for use in coating interferometer fiber sensors: GO and ZnO. Similar to the trend observed with FBG humidity sensors, GO has been more frequently employed as a coating material to enhance sensor performance. The study conducted by Chu et al. [83] using GO reported higher sensitivity, measuring 2.72 nm/RH%, and covered a wider relative humidity (RH) range from 40% to 75% RH. In contrast, the study by Lokman et al. [14] using GO recorded lower sensitivity, at 0.0205 nm/%RH, and had a narrower RH range from 35% to 60% RH. In terms of response time, GO also demonstrated a faster response, with a time of 3.6 s, while studies using ZnO did not specify the exact response time and only mentioned a response time of less than 5 s. Notably, studies employing ZnO as a coating material did not provide information on

recovery time, whereas studies using GO recorded a rapid recovery time of 6.4 s.

C. MICROFIBER RESONATOR

The structures of microfiber resonators are micro-knot (MKR) resonator, micro-loop (MLR) resonator and micro-coil (MCR) resonator. The schematic diagram of these three structures are shown in Fig. 25. The microfiber resonator works based on the resonance effect which the strong evanescent field of microfiber is used to detect the change of the environment medium parameter. The difference in the surrounding medium will affect the RI of the microfiber and will cause a shifting of the resonance wavelength peak in the output spectrum [84].

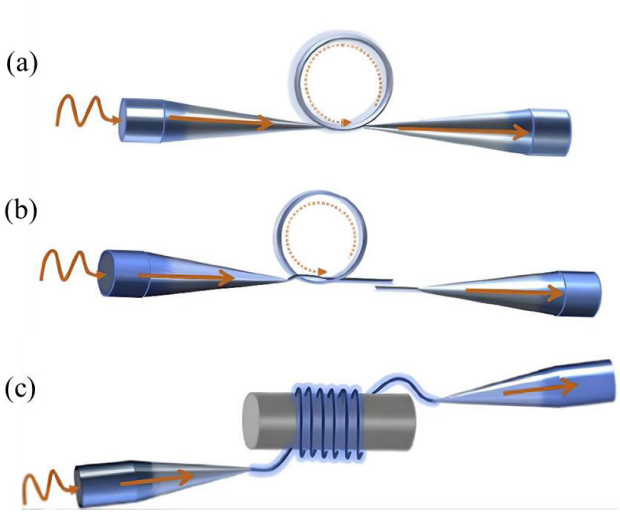

FIGURE 25. Schematic diagram of (a) micro-loop resonator (b) micro-knot resonator and (c) micro-coil resonator [84].

1) MICROFIBER KNOT RESONATOR

The microfiber knot resonator (MKR) presents a more stable structure in comparison to the microfiber loop resonator (MLR) and offers a simpler alternative to the microfiber coil resonator. It demonstrates a reduced susceptibility to external influences [85]. The MKR structure comprises a tapered fiber featuring a waist region ranging from hundred nanometers to several micrometers in diameter, forming a loop. This specific configuration enables the interaction of the evanescent field from the propagating signal with the surrounding environment of the MKR [86]. The fabrication process of the MKR involves utilizing a micro-tapering technique employing various heating sources such as a flame, a laser-based heating tube, or an electric strap heater [87], [88]. The example of a microscopic image of MKR is shown in Fig. 26 (a).

a: SENSING MECHANISM OF MICROFIBER RESONATOR

The working principle of the microfiber resonator is based on the resonance wavelength that will differ as the RH percent varies, resulting in the surrounding RI to change as well. The RI of the material medium relies on its structure and composition, which according to the Lorentz-Lorenz formula, RI can be expressed as the following equation,

$$n = \left(\frac{3M + 8\pi N_A \gamma \rho}{3M - 4\pi N_A \gamma \rho}\right)^{\frac{1}{2}} \tag{15}$$

where n is the RI of the medium, M is the molecular weight of the medium, N_A stands for the Avogadro constant, γ represents the medium's polarization index and ρ denotes the density of the medium [90]. By assuming whole parameters have constant values except the ρ, when the medium expands due to the absorption of the water molecules, the values of ρ and n will decrease. Meanwhile, if the medium shrinks after the absorption process and the interstitial gap in the medium is filled, both ρ and n will increase.

Then, the transmission of light through the microfiber resonator can be estimated by (16), known as coupled-mode equations. The following equation is used to calculate the free spectral range (FSR),

$$FSR \approx \frac{\lambda^2}{N_g \pi D} \approx \frac{\lambda^2}{N_g L} \approx \frac{\lambda^2}{n_{eff} L} \tag{16}$$

where λ is the operating wavelength, N_g is the group index of the mode propagating in the microfiber, n_{eff} is the effective RI of the microfiber, and L is the loop length of either the MKR or the MLR. From (16), any changes in RI or the loop length will cause the resonance wavelength to be shifted. This phenomenon will be supported by the example of the research using MKR and MLR for humidity sensing applications, in the following section.

b: METAL OXIDE COATED MICROFIBER KNOT RESONATOR

Several metal oxides have been discovered and utilized as coating for MKR in humidity sensing applications. Faruki et al. exploited titanium dioxide TiO_2 to increase the humidity sensing performance of the sensor [89]. In their study, the microfiber was fabricated by using the flame brushing method on SMF. After the tapering process, the MKR with a diameter of 2.5 mm is produced, as shown in Fig. 26 (b). The MKR was stationed in the humidity chamber with a light from a tunable laser source (TLS) injected through it, and the MKR output was divided by the 50:50 coupler. The output was then measured by the OSA and optical power meter (OPM). The hygrometer was also being placed inside the humidity chamber as reference RH. The experiment setup of this research is shown in Fig. 26 (c).

This research was first conducted by using uncoated MKR. As the humidity inside the chamber fluctuated, the silica fiber absorbed the water vapor molecule, causing a change in RI. The RI increased with the rise in RH. The water molecule successively increased the density of the fiber and contributed to a positive resonance wavelength shift. The sensitivity of the uncoated MKR was observed to be equal to 0.0013 nm/%RH. The positive shifting trend and sensitivity are illustrated in Fig. 27.

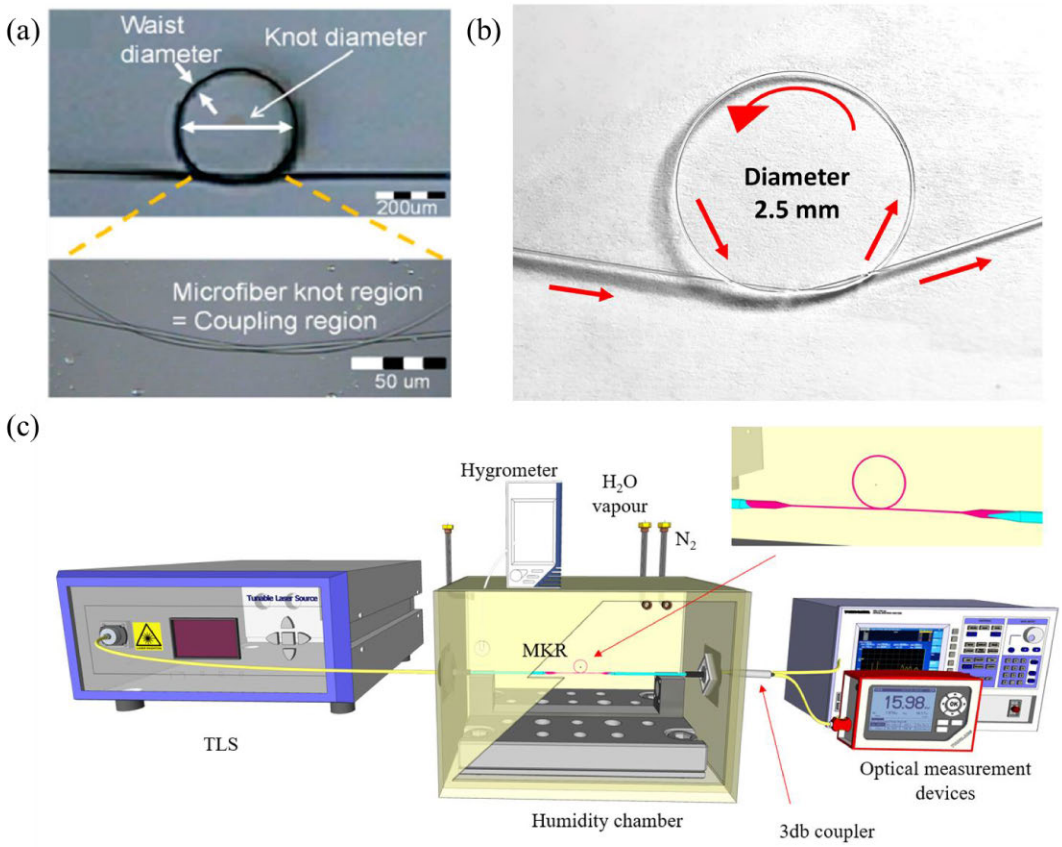

FIGURE 26. (a) Microscopic image of MKR [87]. (b) Schematic diagram of the MKR. (c) Experiment setup for relative humidity sensing using MKR. Adopted from [89].

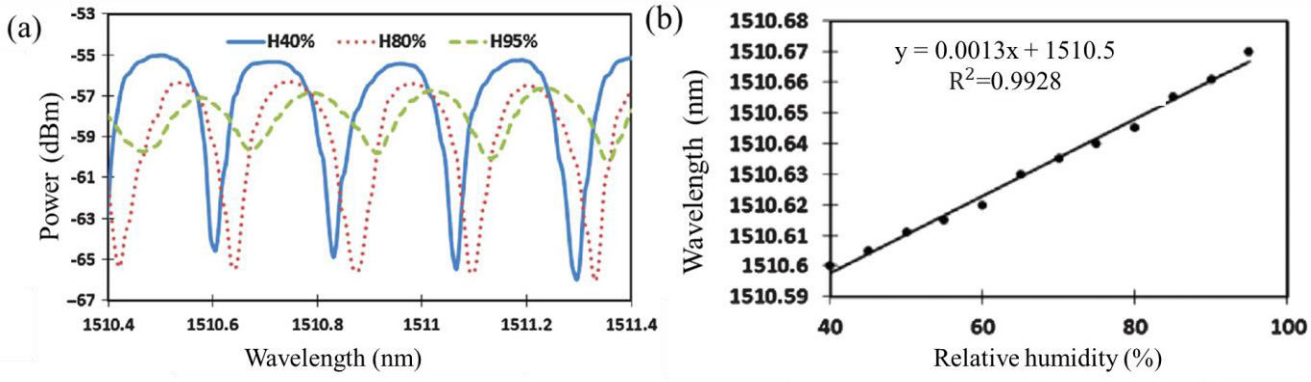

FIGURE 27. Behavior of uncoated MKR (a) transmitted power spectra for three different RH (b) resonance wavelength versus RH [89].

Then, the research was continued using TiO_2 coated MKR. To observe whether the TiO_2 nanoparticles were attached to the microfiber, OPM was used to monitor the light ejected by TLS into the MKR. As the MKR was immersed inside the TiO_2 solution, the loss of light transmission started to rise due to the use of a solvent, DI-water, which evaporated easily. This allowed the attachment of TiO2 nanoparticles to the fiber knot. Other than that, the evanescent field surrounding the knot played a role in attracting and binding the TiO2 nanoparticles to the fiber knot.

The coated MKR was exposed to RH range from 40% to 95%, and it exhibited higher sensitivity than the uncoated MKR. Since the structure of TiO_2 was porous, it assisted the adsorption and capillary condensation to develop as the RH was increased. The RI of the TiO_2 also increased as the water molecules filling up the porous TiO_2. The response of coated MKR to RH increment is presented in Fig. 28 (a).

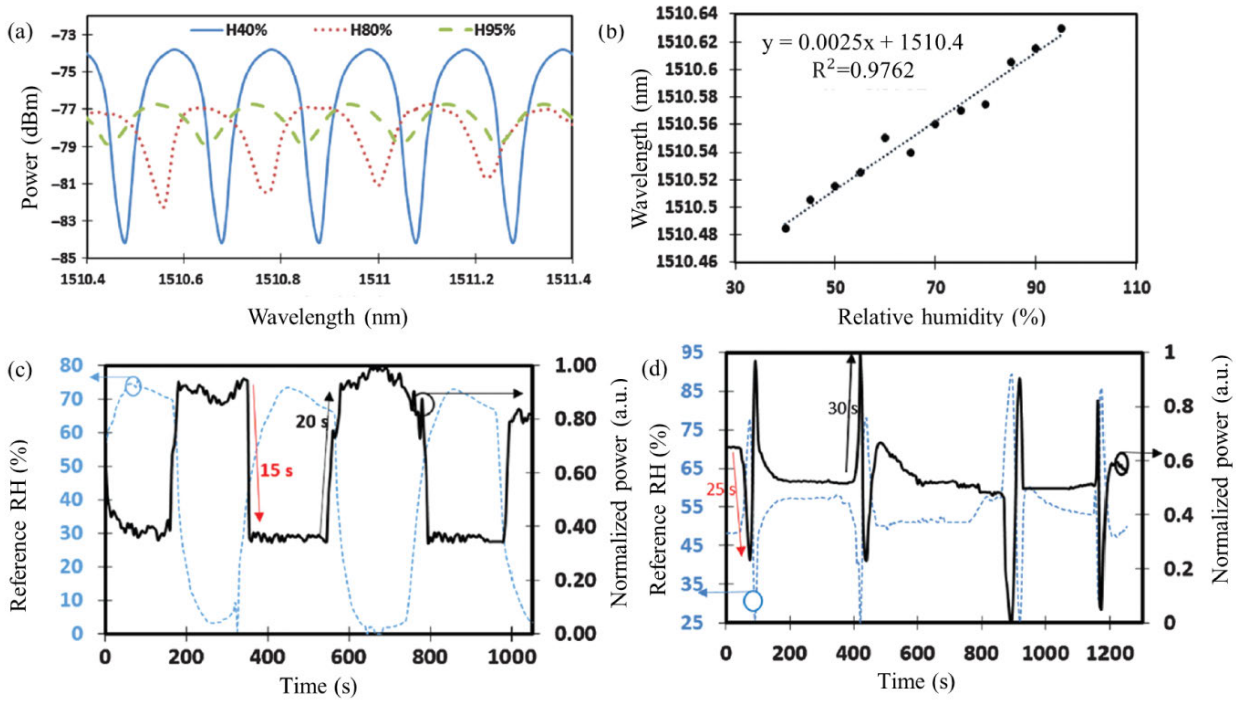

FIGURE 28. Behavior of TiO_2 coated MKR (a) transmitted power spectra for three different RH (b) resonance wavelength versus RH. Response and recovery time of (c) uncoated MKR (d) coated MKR to drastic humidity change [89].

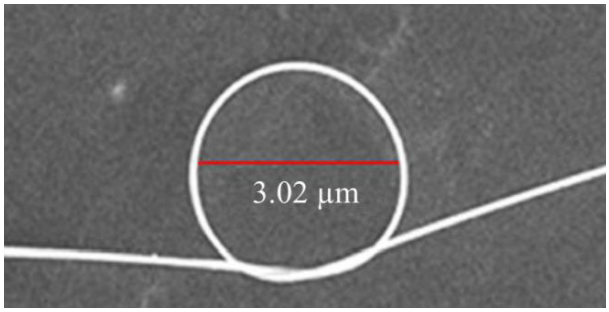

FIGURE 29. Microscope image of fabricated MKR with a diameter of 3.02 μm [86].

Fig. 28 (b) shows the coated MKR response is in linear relationship with the increment of RH from 40% to 95% RH. The sensitivity of MKR increased by 92.30% when coated with TiO_2, with sensitivity recorded at 0.0025 nm/%RH. This was owing to the presence of a nano-scale porous arrangement in the TiO_2 coating, which facilitated greater capacity for efficient adsorption of water molecules compared to the uncoated MKR. The resonance wavelength of the TiO_2 coated MKR also shifted more significantly than the uncoated MKR. The graph for the response and recovery time of uncoated and coated MKR are shown in Fig. 28 (c) and (d). Based on this figure, the response and recovery time for uncoated MKR are 15 s and 20 s while the coated MKR are 25 s and 30 s. The fast response time indicated a fast diffusion process, while the slow recovery time showed a slow desorption process.

Next, Azzuhri et al. used GO coated MKR for humidity applications [86]. GO was employed due to its high sensitivity and the existence of oxygen functional groups such as carboxyl, hydroxyl and epoxy groups in their hexagonal crystalline structure of graphene [91], [92], thus making it easier to handle. Other than that, GO could be easily reduced in solution to form a thin film, making it convenient to be used in coating MKR [93]. The MKR used in this sensing application was fabricated by using the flame-heating technique on a single SMF. Maintaining the core diameter unchanged while thinning the cladding to a point where it becomes exceptionally thin, the core was exposed at the tapered waist region. This facilitated the interaction between the core and the surrounding medium. This research constructed the MKR by looping the fabricated tapered fiber, forming a ring at the tapered region. The microscope image of fabricated MKR with a diameter of 3.02 μm is shown in Fig. 29.

To observe the effect of GO coating on MKR, the research was carried out using both uncoated and coated MKR. The coating process of MKR was completed by drop-casting the GO solution on the MKR. The transmission spectrum of MKR without and with GO coating are shown in Fig. 30 (a) and (b). The transmission spectrum of coated MKR increased from -41 to -27 dBm as the RH was increased.

Meanwhile, for uncoated MKR, the increment of transmission spectrum was only 10 dBm. The analysis on the transmission spectrum revealed that the GO layer exhibited a high level of hygroscopicity, resulting in a higher amount of water molecules being absorbed by the GO layer as the RH%

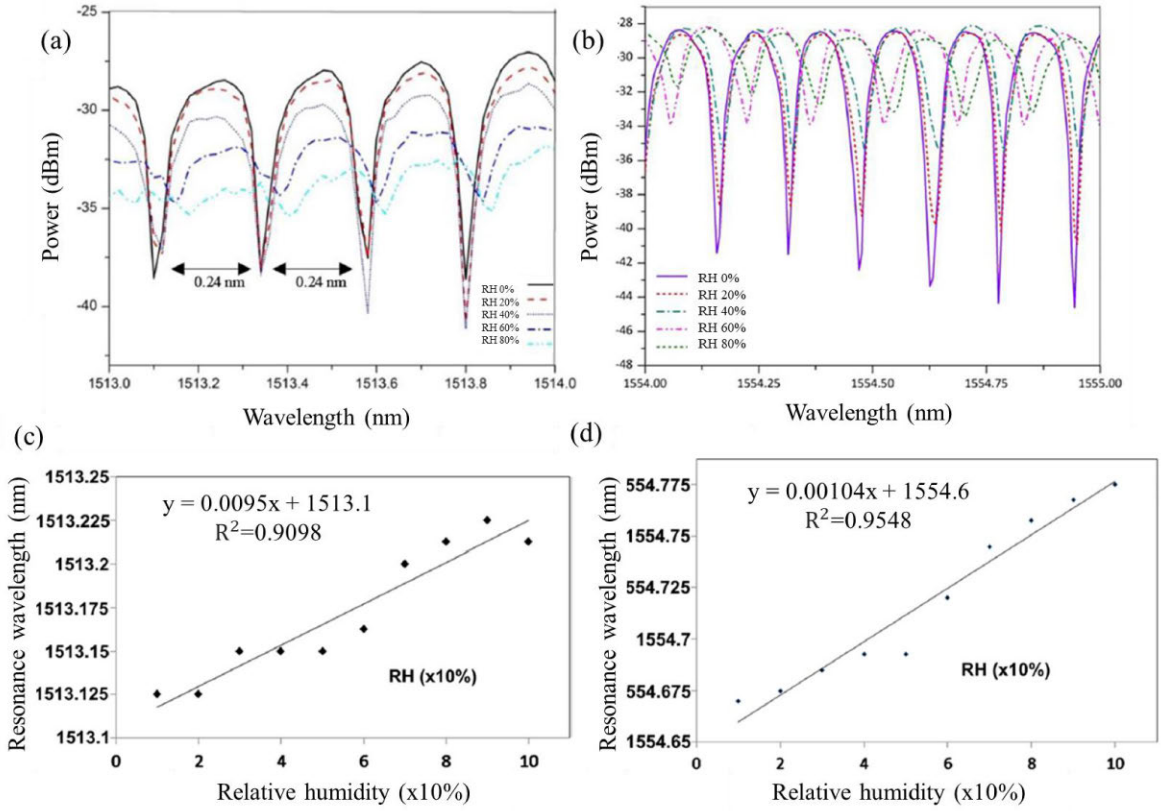

FIGURE 30. Transmission spectrum of MKR (a) without GO coating (b) with GO coating. Resonance wavelength shift versus RH graph for (c) uncoated MKR (d) GO coated MKR [86].

increases. Subsequently, this resulted in a rise will in RI of the GO layer, enhancing its capability to confine the evanescent field of the test signal as it traversed through the core of the MKR. As uncoated MKR, the change of RI was less significant compared to GO coated MKR. The comparison on the resonance wavelength shift between uncoated and GO coated MKR are shown in Fig. 30 (c) and (d).

The graph in Fig. 30 shows the resonance wavelength shift as the RH percent increases for uncoated MKR and coated MKR. The sensitivity for uncoated and coated MKR are analyzed at 0.0095 nm/% RH and 0.0104 nm/% RH, respectively. By comparing these two obtained sensitivity values, it could be proven that GO film was accountable for the increased humidity sensitivity. The existence of oxygen functional groups on GO surface promoted higher adsorption of water molecules on its surface. In this section, it can be summarized there were two types of metal oxide used in coating the MKR, which were TiO_2 and GO. The research using GO showed significantly higher sensitivity for humidity, with sensitivity four times greater than the sensitivity of TiO_2 coated MKR. However, when considering response and recovery times, the study conducted by Faruki et. al which utilized TiO_2, recorded 25 s for response time and 35 s for recovery time. The remarkable aspect of GO is its broad RH detection range, spanning from 0% to 80% RH, making it suitable for wide range of applications, encompassing from low percentage to high percentage RH.

2) MICROFIBER LOOP RESONATOR

Microfiber loop resonator (MLR) is one of the microfiber resonator structures that only has a single turn of microfiber coil [94]. MLR is fabricated by tapering an optical fiber to the required diameter, followed by the formation a self-touching loop that is supported by the static electricity and Van der Waals forces. The coupling efficiency of the loop can be enhanced by changing the tapering process carefully. MLR structure is reactive to humidity changes in the surrounding environment because of the evanescent mode around the loop, which is very sensitive to RH changes [95]. An example of the schematic MLR structure is shown in Fig. 31 (a). In addition to the aforementioned advantages of MLR, it is also easy to fabricate and has chemical stability, simple structure and has low insertion loss thus making it convenient to be used in sensing application [95].

a: METAL OXIDE COATED MICROFIBER LOOP RESONATOR FOR HUMIDITY SENSING

Two undertaken research studies that were conducted employed ZnO as the coating material for MKR to increase the sensitivity. This semiconductor metal oxide has good

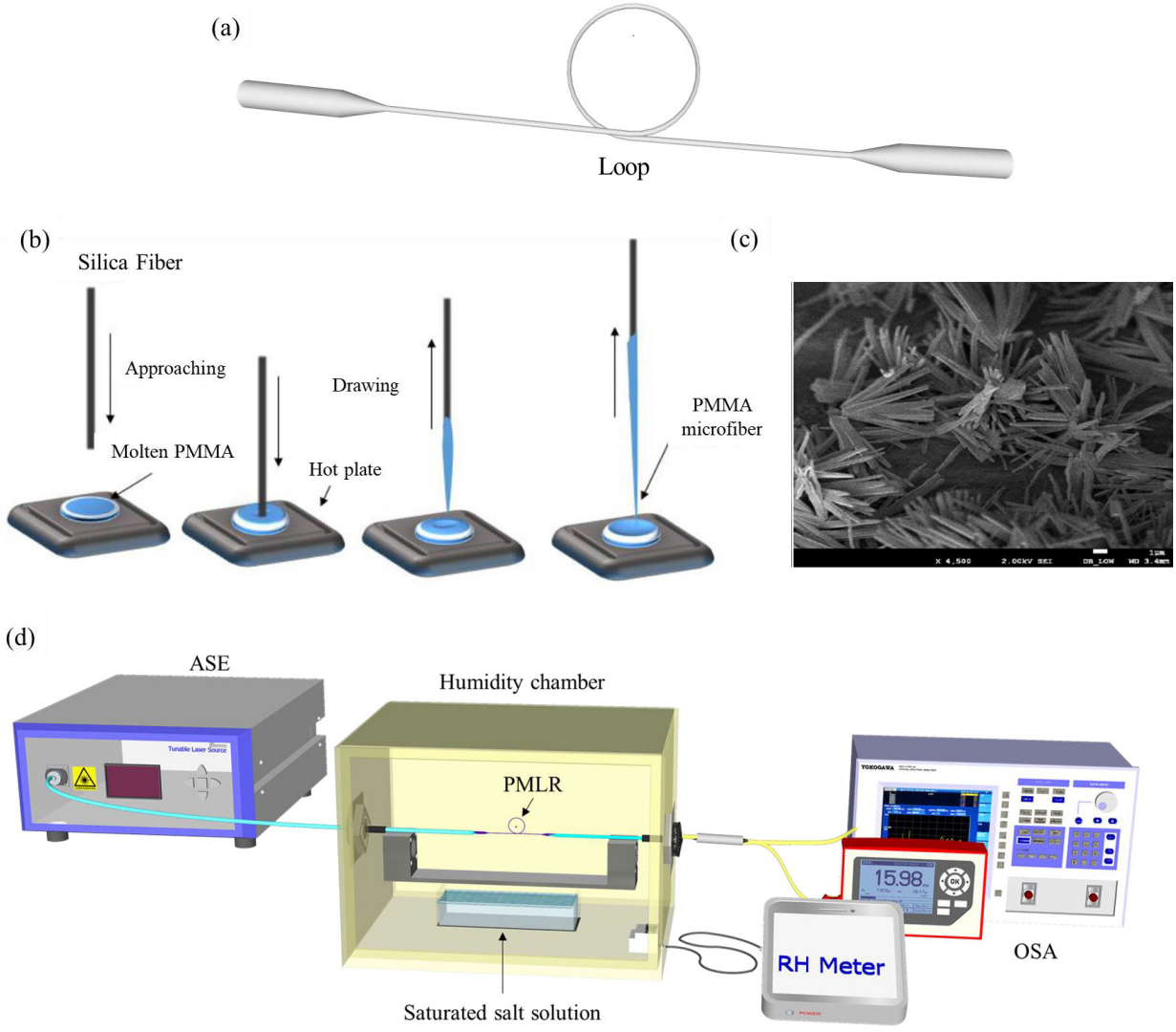

FIGURE 31. (a) Schematic diagram of MLR structure. Adopted from [96]. (b) Fabrication process of PMMA microfiber. (c) FESEM images of 4500x magnified image of ZnO nanorods. (d) Experiment setup for relative humidity sensing using uncoated and ZnO coated PMLR. Adopted from [97].

electrical and optical properties suitable for sensing applications. Other than improved sensing performance, ZnO was used as the sensing material due to its huge surface area, low cost, and bio-safe properties [95], [98], [99]. The first research was conducted in 2017 by using a Polymethyl methacrylate (PMMA) microfiber loop resonator (PMLR) coated with zinc oxide (ZnO) nanorods [97]. In this research, a bent 8 μm diameter of PMMA microfiber with a loop diameter of 42 μm was used for RH sensing. The PMMA microfiber was produced using a molten PMMA in conjunction with the direct drawing technique. This technique involved the use of hot plate to melt the PMMA and ensured the temperature was also maintained. The fabrication process is shown in Fig. 31 (b).

The fabrication process started by immersing the tip of the silica fiber into the molten PMMA. Next, the fiber tip was drawn and the molten PMMA was extended, resulting in the formation of a bare PMMA microfiber upon cooling in the surrounding air. Then, the ZnO nanorods were coated onto the fiber using the sol-gel immersion method.

To observe the growth of ZnO nanorods on the PMMA, FESEM was used, and the microscopic images are shown in Fig. 31 (c). From the FESEM image, the ZnO nanorods were observed to be scattered, but their diameters and length were uniforms. To investigate the RH sensing of the PMLR, the PMLR was placed inside the humidity chamber with a range of 50% to 80% RH. Then, a light source from ASE was ejected into the coated and uncoated PMLR. Next, the

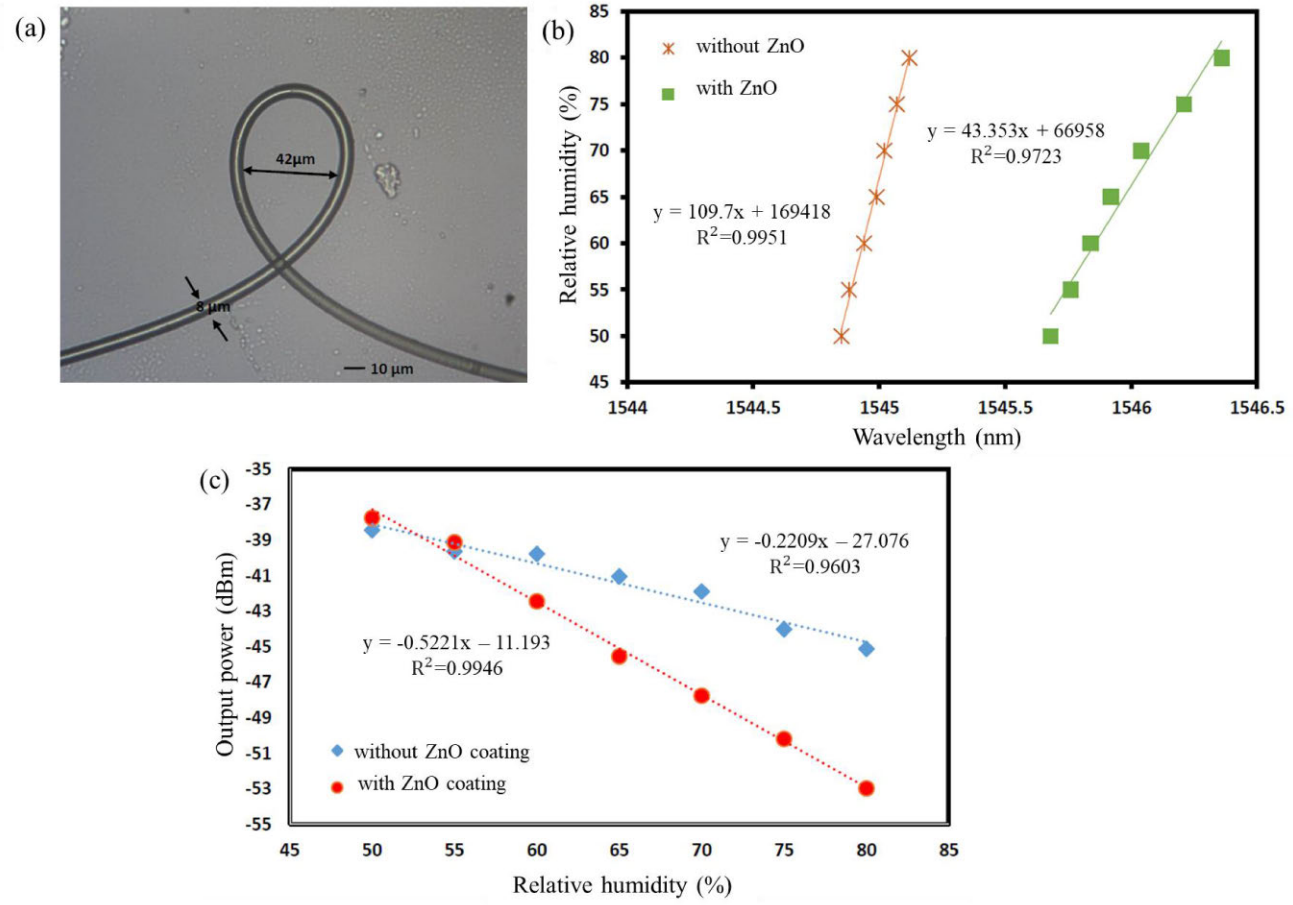

FIGURE 32. (a) Microscopic image of PMLR. (b) Relative humidity response to uncoated and ZnO coated PMLR. (c) Output power versus relative humidity for uncoated and ZnO coated PMLR [97].

transmitted light and the wavelength shift was measured using OSA. The experiment setup of this research is shown in Fig. 31 (d) and the microscopic image of PMLR with 4000x magnification is shown in Fig. 32 (a).

From Fig. 32 (a) the microfiber loop structure is maintained by the Van der Waals attraction force that connects the two neighboring PMMA microfibers. This attraction was strong enough to stand the elastic force from the bent microfiber. The relative humidity versus resonant wavelength shift of the uncoated and ZnO-coated PMLR is shown in Fig. 32 (b). From Fig. 32 (b) the wavelength is gradually shifted from 50% to 80% RH for both uncoated and coated PMLR. From this graph, the sensitivity of ZnO coated PMLR is observed to be equal to 0.0224 nm/%RH and the uncoated PMLR has lower sensitivity at 0.0091 nm/%RH. Then, the transmitted light from the PMLR versus various RH level results is illustrated in Fig. 32 (c). From the graph, the transmitted light of ZnO coated PMLR decreases with increasing RH with the sensitivity of 0.5221 dBm/%RH. From this research, by coating the PMLR with ZnO nanorods, it was proven the performance of the sensor can be enhanced. As the ZnO layer absorbed the water molecules, the RI of the effective coating of the fiber was increased. The increment of RI resulted in a greater leakage of light and induced an extra mass on the surface, influencing the transmission characteristics of the PMLR.

The second research was conducted in 2020 by Adnan Zain et al. using ZnO nanorods coated MLR for RH sensing [95]. The sensing mechanism of this sensor was highly dependent on the dispersion of the evanescent mode surrounding the looped section. Alterations in RI of the nearby surroundings notably affected this evanescent wave. The schematic diagram of MLR used in this research is shown in Fig. 33. When the RH increased, the ZnO absorbed a higher amount of water, causing more light to refract into the coating layer. This led to a decrease in the light intensity inside the MLR, resulting in significant transmission loss. Therefore, the output power linearly decreased as RH increased, producing higher sensitivity than the uncoated MLR structure.

The silica fiber was tapered to the desired diameter of 7 μm by using the flame brushing technique. Next, the tapered fiber was circled into a self-touching loop with a diameter of 300 μm as depicted in Fig. 34 (a).

TABLE 3. Sensing performance of metal oxide coated microfiber resonator.

Sensing Technique	Sensing Material	Coating Technique	Sensitivity	Response Time	Recovery Time	Reference
Microfiber knot resonator (MKR)	Titanium dioxide, TiO_2	Dip coating	0.0025 nm/%RH (40% to 95% RH)	15 s	20 s	[89]
	Graphene Oxide, GO	Drop casting	0.0104 nm/%RH (0% to 80% RH)	N/A	N/A	[86]
Microfiber loop resonator (MLR)	Zinc Oxide, ZnO	Dip coating	0.5221 dBm/%RH (50 % to 80% RH)	N/A	N/A	[97]
		Sol gel method	0.2774 dBm/%RH (35% to 85% RH)	0.744 s	1.04 s	[95]

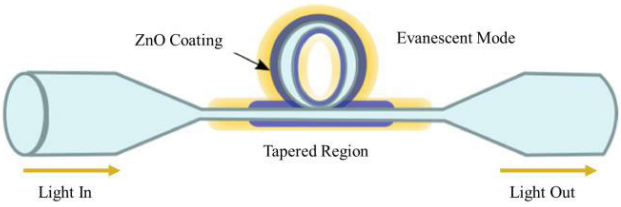

FIGURE 33. Schematic diagram of MLR coated ZnO [95].

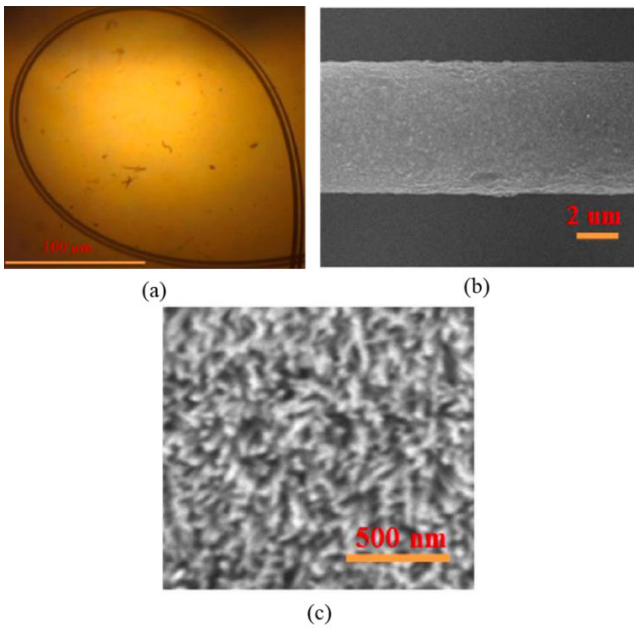

FIGURE 34. (a) Microscopic image of MLR. (b) FESEM image of ZnO on the MLR at 5 kx magnification and (c) 10.00 kx magnification [95].

Then, the tapered fiber was immersed into ZnO solution prepared using the sol-gel method. To verify the successful growth of ZnO nanorods on the MLR, FESEM was used to study its morphology. The FESEM images of ZnO-coated MLR are shown in Fig. 34 (b) and (c). The light propagation inside this sensor was examined by emitting the light source from TLS, recording the output power using OPM, and connecting it to a computer to observe the power spectrum.

The fiber sample was positioned inside the humidity chamber to measure its response time as RH varied from 35% to 85% RH. The response time of the ZnO coated MLR was 0.744 s, faster than the uncoated MLR, with a response time of 1.66 s. The recovery time of this sensor was also quicker at 1.04 s, while uncoated MLR recorded 1.588 s. Fast response and recovery time of the sensor were essential for responding to sudden changes in RH. The graph of output power versus RH is shown in Fig. 35.

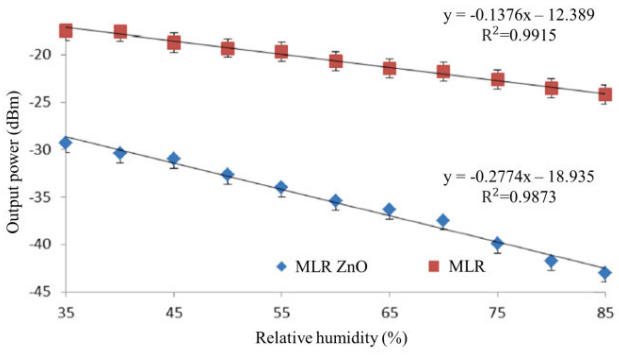

FIGURE 35. Response of uncoated and ZnO coated MLR toward 35% to 85% RH [95].

From Fig. 35, the sensitivity of ZnO coated MLR is 0.2774 dBm/%RH which is two times higher than uncoated MLR, 0.1376 dBm/%RH. The sensitivity of ZnO coated MLR was higher because the power loss increased gradually due to the increment of RI of the ZnO as RH rised. ZnO

absorbed more light from the evanescent mode as the RH increased, resulting in reduction of light propagation inside the ZnO-coated MLR structure. This research successfully demonstrated that by using ZnO as coating material, the response and recovery time and sensor sensitivity were better than the uncoated MLR. Although both works used ZnO, there was a difference in sensitivity which; the ZnO coated PMLR attained higher sensitivity at 0.5221 dBm/%RH. The summary table for microfiber resonator coated with different metal oxides is presented in Table 3.

As shown in Table 3, three types of metal oxides have been identified for use as coating materials in microfiber resonator humidity sensing applications: TiO_2, GO, and ZnO. Due to variations in sensitivity units, it is possible to compare the sensing performance of TiO_2 and GO coatings. A study conducted by Azzuhri et al. [86] used GO as a coating for microfiber resonators (MKR) and achieved a high sensitivity of 0.0104 nm/%RH. This sensitivity was four times higher than that of TiO_2-coated MKR. The broader relative humidity (RH) range covered by the GO-coated MKR makes it suitable for applications where both low and high RH ranges are of primary concern. However, the study by Azzuhri et al. [86] did not investigate the response and recovery times for comparison with TiO_2. Regarding the sensing performance of ZnO-coated microfiber resonators (MLR), both studies on MLR used ZnO, but they employed different deposition techniques. The study by Irawati et al. [97] achieved a high sensitivity of 0.5221 dBm/%RH but with a limited RH range (50% to 80% RH). In contrast, the study by Adnan Zain et al. [95] covered a broader RH range (35% to 85% RH) but recorded a sensitivity of 0.2774 dBm/%RH. Unfortunately, just as with the GO-coated MKR study, the study by Irawati et al. did not investigate response and recovery times, making direct comparisons challenging.

III. CONCLUSION

In conclusion, this paper comprehensively summarizes various methods to monitor relative humidity using optical fiber sensors. This work reviews the working principles of OFHS based on FBG, interferometers, and microfiber resonators in detail. Additionally, several metal oxides have been discussed as sensing materials for each mentioned OFHS, including TiO_2, ZnO, and GO. It is evident from this review that the sensitivity, response, and recovery time of OFHS have shown significant improvement due to the utilization of metal oxide coatings. However, this review has also identified a limitation in the variation of metal oxides employed as coating materials for optical fiber humidity sensors, as only three types have been uncovered. Despite this limitation, this paper has highlighted GO and ZnO as promising candidates due to their high sensitivity, quick response, and recovery times.

From the study on published work, GO is used consistently for all three types of OFHS that are covered in this review. Graphene oxide succeeds in proving its ability to increase the sensitivity of OFHS as it consists of a large number of oxygen-containing groups on the surface and edge that can permeate and absorb water molecules [100]. Besides that, GO can be easily dispersed in solution and can be used as a thin film without requiring sophisticated equipment. Although GO has shown excellent performance on humidity sensing, it is still possible to enhance its performance based on the following suggestions. The first suggestion is to use a combination of 2D materials such as the composition of metal and metal oxide as the sensing material. Other than that, the use of 3D structures instead of 2D structures is proposed to increase the surface area, so that more water molecules to be easily absorbed. It can be achieved by using metal oxide with carbon materials, which are multi-functional nanomaterials that are widely used these days. Even though these two recommendations are already widely used for humidity sensing, their application on optical fiber substrate has gained significant attention only in recent years. Thus, there is still room for improvement where future work can be focused on this area to optimize the fabrication process, further enhance sensing performance and to explore novel sensing mechanisms.

REFERENCES

[1] C. Lin, H. Zhang, J. Zhang, and C. Chen, "Enhancement of the humidity sensing performance in Mg-doped hexagonal ZnO microspheres at room temperature," *Sensors*, vol. 19, no. 3, p. 519, Jan. 2019, doi: 10.3390/s19030519.

[2] X. Zhang, D. Maddipatla, A. K. Bose, S. Hajian, B. B. Narakathu, J. D. Williams, M. F. Mitchell, and M. Z. Atashbar, "Printed carbon nanotubes-based flexible resistive humidity sensor," *IEEE Sensors J.*, vol. 20, no. 21, pp. 12592–12601, Nov. 2020, doi: 10.1109/JSEN.2020.3002951.

[3] S. Khillar. (Jun. 10, 2019). *Difference Between Absolute and Relative Humidity | Difference Between*. Accessed: May 5, 2021. [Online]. Available: http://www.differencebetween.net/science/nature/difference-between-absolute-and-relative-humidity/

[4] E. De Angelis, S. Renzetti, M. Volta, F. Donato, S. Calza, D. Placidi, R. G. Lucchini, and M. Rota, "COVID-19 incidence and mortality in Lombardy, Italy: An ecological study on the role of air pollution, meteorological factors, demographic and socioeconomic variables," *Environ. Res.*, vol. 195, Apr. 2021, Art. no. 110777, doi: 10.1016/j.envres.2021.110777.

[5] R. Ade and M. Rehm, "Is green certification the solution to substandard indoor air quality (humidity)? A case study of old, new and green-certified dwellings," *Australas. J. Environ. Manage.*, vol. 28, no. 2, pp. 126–148, Apr. 2021, doi: 10.1080/14486563.2021.1924300.

[6] H. Farahani, R. Wagiran, and M. Hamidon, "Humidity sensors principle, mechanism, and fabrication technologies: A comprehensive review," *Sensors*, vol. 14, no. 5, pp. 7881–7939, Apr. 2014, doi: 10.3390/s140507881.

[7] P. Jagdale, D. Ziegler, M. Rovere, J. Tulliani, and A. Tagliaferro, "Waste coffee ground biochar: A material for humidity sensors," *Sensors*, vol. 19, no. 4, p. 801, Feb. 2019, doi: 10.3390/s19040801.

[8] S. Khasim, A. Pasha, N. Badi, M. Lakshmi, S. A. Al-Ghamdi, and H. A. AL-Aoh, "PVA treated PEDOT-PSS: TiO_2 nanocomposite based high-performance sensors towards detection of relative humidity and soil moisture content for agricultural applications," *J. Polym. Environ.*, vol. 29, no. 2, pp. 612–623, Feb. 2021, doi: 10.1007/s10924-020-01905-6.

[9] G. Guarnieri, B. Olivieri, G. Senna, and A. Vianello, "Relative humidity and its impact on the immune system and infections," *Int. J. Mol. Sci.*, vol. 24, no. 11, p. 9456, May 2023, doi: 10.3390/ijms24119456.

[10] R. Correia, S. James, S.-W. Lee, S. P. Morgan, and S. Korposh, "Biomedical application of optical fibre sensors," *J. Opt.*, vol. 20, no. 7, Jun. 2018, Art. no. 073003, doi: 10.1088/2040-8986/aac68d.

[11] S. Tonello, M. Borghetti, E. Sardini, and M. Serpelloni, "Improved portable measuring device for real-time humidity and temperature monitoring in intensive care unit," *IEEE Instrum. Meas. Mag.*, vol. 23, no. 4, pp. 79–86, Jun. 2020, doi: 10.1109/MIM.2020.9126076.

[12] F. U. Hernandez, S. P. Morgan, B. R. Hayes-Gill, D. Harvey, W. Kinnear, A. Norris, D. Evans, J. G. Hardman, and S. Korposh, "Characterization and use of a fiber optic sensor based on PAH/SiO_2 film for humidity sensing in ventilator care equipment," *IEEE Trans. Biomed. Eng.*, vol. 63, no. 9, pp. 1985–1992, Sep. 2016, doi: 10.1109/TBME.2016.2521662.

[13] Y.-D. Chiu, C.-W. Wu, and C.-C. Chiang, "Tilted fiber Bragg grating sensor with graphene oxide coating for humidity sensing," *Sensors*, vol. 17, no. 9, p. 2129, Sep. 2017, doi: 10.3390/s17092129.

[14] A. Lokman, H. Arof, S. W. Harun, Z. Harith, H. A. Rafaie, and R. M. Nor, "Optical fiber relative humidity sensor based on inline Mach–Zehnder interferometer with ZnO nanowires coating," *IEEE Sensors J.*, vol. 16, no. 2, pp. 312–316, Jan. 2016, doi: 10.1109/JSEN.2015.2431716.

[15] T. Delipinar, A. Shafique, M. S. Gohar, and M. K. Yapici, "Fabrication and materials integration of flexible humidity sensors for emerging applications," *ACS Omega*, vol. 6, no. 13, pp. 8744–8753, Apr. 2021, doi: 10.1021/acsomega.0c06106.

[16] T. S. E. F. Karunarathne, W. P. S. L. Wijesinghe, N. P. W. Rathuwadu, A. Karalasingam, N. Manoharan, S. A. L. Sameera, C. Sandaruwan, G. A. Amaratunga, and S. G. M. de Silva, "Fabrication and characterization of partially conjugated poly (vinyl alcohol) based resistive humidity sensor," *Sens. Actuators A, Phys.*, vol. 314, Oct. 2020, Art. no. 112263, doi: 10.1016/j.sna.2020.112263.

[17] L. Alwis, T. Sun, and K. T. V. Grattan, "Optical fibre-based sensor technology for humidity and moisture measurement: Review of recent progress," *Measurement*, vol. 46, no. 10, pp. 4052–4074, Dec. 2013, doi: 10.1016/J.MEASUREMENT.2013.07.030.

[18] J. Ascorbe, J. Corres, F. Arregui, and I. Matias, "Recent developments in fiber optics humidity sensors," *Sensors*, vol. 17, no. 4, p. 893, Apr. 2017, doi: 10.3390/s17040893.

[19] J. Ascorbe, J. Corres, F. Arregui, and I. Matias, "Humidity sensor based on Bragg gratings developed on the end facet of an optical fiber by sputtering of one single material," *Sensors*, vol. 17, no. 5, p. 991, Apr. 2017, doi: 10.3390/s17050991.

[20] X. Rao, L. Zhao, L. Xu, Y. Wang, K. Liu, Y. Wang, G. Y. Chen, T. Liu, and Y. Wang, "Review of optical humidity sensors," *Sensors*, vol. 21, no. 23, p. 8049, Dec. 2021, doi: 10.3390/s21238049.

[21] Y. Zhong, P. Xu, J. Yang, and X. Dong, "Optical fiber interferometric humidity sensor by using hollow core fiber interacting with gelatin film," *Sensors*, vol. 22, no. 12, p. 4514, Jun. 2022, doi: 10.3390/s22124514.

[22] Y. R. Herrero and A. Ullah, "Metal oxide powder technologies in catalysis," in *Metal Oxide Powder Technologies*. Amsterdam, The Netherlands: Elsevier, 2020, pp. 279–297, doi: 10.1016/b978-0-12-817505-7.00014-2.

[23] C. H. Voon, K. L. Foo, B. Y. Lim, S. C. B. Gopinath, and Y. Al-Douri, "Synthesis and preparation of metal oxide powders," in *Metal Oxide Powder Technologies*. Amsterdam, The Netherlands: Elsevier, 2020, pp. 31–65, doi: 10.1016/b978-0-12-817505-7.00003-8.

[24] D. Zhang, Z. Yang, S. Yu, Q. Mi, and Q. Pan, "Diversiform metal oxide-based hybrid nanostructures for gas sensing with versatile prospects," *Coordination Chem. Rev.*, vol. 413, Jun. 2020, Art. no. 213272, doi: 10.1016/j.ccr.2020.213272.

[25] L.-X. Ou, M.-Y. Liu, L.-Y. Zhu, D. W. Zhang, and H.-L. Lu, "Recent progress on flexible room-temperature gas sensors based on metal oxide semiconductor," *Nano-Micro Lett.*, vol. 14, no. 1, p. 206, Oct. 2022, doi: 10.1007/s40820-022-00956-9.

[26] H. Yu, C. Guo, X. Zhang, Y. Xu, X. Cheng, S. Gao, and L. Huo, "Recent development of hierarchical metal oxides based gas sensors: From gas sensing performance to applications," *Adv. Sustain. Syst.*, vol. 6, no. 4, Apr. 2022, Art. no. 2100370, doi: 10.1002/adsu.202100370.

[27] A. Dey, "Semiconductor metal oxide gas sensors: A review," *Mater. Sci. Eng., B*, vol. 229, pp. 206–217, Mar. 2018, doi: 10.1016/j.mseb.2017.12.036.

[28] R. Viter and I. Iatsunskyi, "Metal oxide nanostructures in sensing," in *Nanomaterials Design for Sensing Applications*. Amsterdam, The Netherlands: Elsevier, 2019, pp. 41–91, doi: 10.1016/B978-0-12-814505-0.00002-3.

[29] M. S. Chavali and M. P. Nikolova, "Metal oxide nanoparticles and their applications in nanotechnology," *Social Netw. Appl. Sci.*, vol. 1, no. 6, p. 607, Jun. 2019, doi: 10.1007/s42452-019-0592-3.

[30] N. Goel, K. Kunal, A. Kushwaha, and M. Kumar, "Metal oxide semiconductors for gas sensing," *Eng. Rep.*, vol. 5, no. 6, Jun. 2023, Art. no. e12604, doi: 10.1002/eng2.12604.

[31] M. Li, Z.-X. Jin, W. Zhang, Y.-H. Bai, Y.-Q. Cao, W.-M. Li, D. Wu, and A.-D. Li, "Comparison of chemical stability and corrosion resistance of group IV metal oxide films formed by thermal and plasma-enhanced atomic layer deposition," *Sci. Rep.*, vol. 9, no. 1, Jul. 2019, Art. no. 10438, doi: 10.1038/s41598-019-47049-z.

[32] D. Nunes, A. Pimentel, A. Gonçalves, S. Pereira, R. Branquinho, P. Barquinha, E. Fortunato, and R. Martins, "Metal oxide nanostructures for sensor applications," *Semicond. Sci. Technol.*, vol. 34, no. 4, Mar. 2019, Art. no. 043001, doi: 10.1088/1361-6641/ab011e.

[33] P. Singh and S. K. Shukla, "Structurally optimized cupric oxide/polyaniline nanocomposites for efficient humidity sensing," *Surf. Interfaces*, vol. 18, Mar. 2020, Art. no. 100410, doi: 10.1016/j.surfin.2019.100410.

[34] G. Hegde, S. Asokan, and G. Hegde, "Fiber Bragg grating sensors for aerospace applications: A review," *ISSS J. Micro Smart Syst.*, vol. 11, no. 1, pp. 257–275, Jun. 2022, doi: 10.1007/s41683-022-00101-z.

[35] N. Abdukerim, D. Grobnic, C. Hnatovsky, and S. J. Mihailov, "Through-the-coating writing of tilted fiber Bragg gratings with the phase mask technique," *Opt. Exp.*, vol. 27, no. 26, p. 38259, Dec. 2019, doi: 10.1364/oe.27.038259.

[36] B. Jiang and J. Zhao, "Nanomaterial-functionalized tilted fiber gratings for optical modulation and sensing," *J. Lightw. Technol.*, vol. 41, no. 13, pp. 4103–4113, Jul. 1, 2023, doi: 10.1109/JLT.2022.3216728.

[37] L. Fazzi and R. M. Groves, "Demodulation of a tilted fibre Bragg grating transmission signal using α-shape modified Delaunay triangulation," *Measurement*, vol. 166, Dec. 2020, Art. no. 108197, doi: 10.1016/j.measurement.2020.108197.

[38] B. Jiang, Z. Bi, Z. Hao, Q. Yuan, D. Feng, K. Zhou, L. Zhang, X. Gan, and J. Zhao, "Graphene oxide-deposited tilted fiber grating for ultrafast humidity sensing and human breath monitoring," *Sens. Actuators B, Chem.*, vol. 293, pp. 336–341, Aug. 2019, doi: 10.1016/j.snb.2019.05.024.

[39] W. Zhang, L. Zhu, M. Dong, X. Lou, and F. Liu, "A temperature fiber sensor based on tapered fiber Bragg grating fabricated by femtosecond laser," *Appl. Sci.*, vol. 8, no. 12, p. 2616, Dec. 2018, doi: 10.3390/app8122616.

[40] O. de la Torre, I. Floris, S. Sales, and X. Escaler, "Fiber Bragg grating sensors for underwater vibration measurement: Potential hydropower applications," *Sensors*, vol. 21, no. 13, p. 4272, Jun. 2021, doi: 10.3390/s21134272.

[41] J. K. Sahota, N. Gupta, and D. Dhawan, "Fiber Bragg grating sensors for monitoring of physical parameters: A comprehensive review," *Opt. Eng.*, vol. 59, no. 6, Jun. 2020, Art. no. 060901, doi: 10.1117/1.oe.59.6.060901.

[42] A. Malakzadeh, M. Mansoursamaei, and R. Pashaie, "Simultaneous measurement of temperature and strain based on peak power changes and wavelength shift using only one uniform fiber Bragg grating," *Opt. Quantum Electron.*, vol. 53, no. 5, p. 208, Apr. 2021, doi: 10.1007/S11082-021-02865-4.

[43] C. N. Macambira, P. G. Der Agopian, J. A. Martino, H. Hadano, A. Miyagi, T. Okuno, M. Mori, Y. Sadaoka, T. Ueda, and S. Qiao, "Humidity sensor based on fiber grating coated with graphene oxide," *J. Phys., Conf. Ser.*, vol. 1213, no. 4, Jun. 2019, Art. no. 042076, doi: 10.1088/1742-6596/1213/4/042076.

[44] J. Zhang, X. Shen, M. Qian, Z. Xiang, and X. Hu, "An optical fiber sensor based on polyimide coated fiber Bragg grating for measurement of relative humidity," *Opt. Fiber Technol.*, vol. 61, Jan. 2021, Art. no. 102406, doi: 10.1016/j.yofte.2020.102406.

[45] Z. Xie, H. Yan, Y. Li, and X. Zhao, "A humidity fiber sensor based on both end-sides of a fiber Bragg grating coated with polyimide," *Opt. Fiber Technol.*, vol. 57, Jul. 2020, Art. no. 102220, doi: 10.1016/j.yofte.2020.102220.

[46] C. Hong, Y. Yuan, Y. Yang, Y. Zhang, and Z. A. Abro, "A simple FBG pressure sensor fabricated using fused deposition modelling process," *Sens. Actuators A, Phys.*, vol. 285, pp. 269–274, Jan. 2019, doi: 10.1016/j.sna.2018.11.024.

[47] W. Zhang, X. Lang, X. Liu, G. Li, R. Singh, B. Zhang, and S. Kumar, "Advances in tapered optical fiber sensor structures: From conventional to novel and emerging," *Biosensors*, vol. 13, no. 6, p. 644, Jun. 2023, doi: 10.3390/bios13060644.

[48] S. Korposh, S. James, S.-W. Lee, and R. Tatam, "Tapered optical fibre sensors: Current trends and future perspectives," *Sensors*, vol. 19, no. 10, p. 2294, May 2019, doi: 10.3390/s19102294.

[49] S. Yu, H. Zhang, C. Lin, and M. Bian, "The enhancement of humidity sensing performance based on Eu-doped ZnO," *Current Appl. Phys.*, vol. 19, no. 2, pp. 82–88, Feb. 2019, doi: 10.1016/j.cap.2018.11.015.

[50] R. Sha, A. Basak, P. C. Maity, and S. Badhulika, "ZnO nanostructured based devices for chemical and optical sensing applications," *Sensors Actuators Rep.*, vol. 4, Nov. 2022, Art. no. 100098, doi: 10.1016/j.snr.2022.100098.

[51] S. Yu, H. Zhang, C. Chen, and C. Lin, "Investigation of humidity sensor based on Au modified ZnO nanosheets via hydrothermal method and first principle," *Sens. Actuators B, Chem.*, vol. 287, pp. 526–534, May 2019, doi: 10.1016/j.snb.2019.02.089.

[52] H. Zhang, S. Yu, C. Chen, J. Zhang, J. Liu, and P. Li, "Effects on structure, surface oxygen defects and humidity performance of Au modified ZnO via hydrothermal method," *Appl. Surf. Sci.*, vol. 486, pp. 482–489, Aug. 2019, doi: 10.1016/j.apsusc.2019.04.266.

[53] W. Gu, H. Zhang, C. Chen, and J. Zhang, "Study on the design of ZnO/PANI composites and the mechanism of enhanced humidity sensing properties," *Current Appl. Phys.*, vol. 34, pp. 112–121, Feb. 2022, doi: 10.1016/j.cap.2021.11.013.

[54] A. M. Aris, H. A. Rahman, N. Irawati, S. W. Harun, and S. S. Sarnin, "Tapered fiber Bragg grating sensor coated with zinc oxide nanostructures for humidity measurement," *J. Telecommun., Electron. Comput. Eng.*, vol. 9, nos. 1–5, pp. 1–5, Apr. 2017. Accessed: Oct. 21, 2021. [Online]. Available: https://jtec.utem.edu.my/jtec/article/view/1822

[55] F. Esposito, L. Sansone, A. Srivastava, F. Baldini, S. Campopiano, F. Chiavaioli, M. Giordano, A. Giannetti, and A. Iadicicco, "Long period grating in double cladding fiber coated with graphene oxide as high-performance optical platform for biosensing," *Biosensors Bioelectron.*, vol. 172, Jan. 2021, Art. no. 112747, doi: 10.1016/j.bios.2020.112747.

[56] F. Esposito, L. Sansone, A. Srivastava, A. M. Cusano, S. Campopiano, M. Giordano, and A. Iadicicco, "Label-free detection of vitamin D by optical biosensing based on long period fiber grating," *Sens. Actuators B, Chem.*, vol. 347, Nov. 2021, Art. no. 130637, doi: 10.1016/j.snb.2021.130637.

[57] F. Esposito, S. Campopiano, and A. Iadicicco, "Arc-induced long period gratings in Erbium-doped fiber," *IEEE Photon. J.*, vol. 11, no. 1, pp. 1–8, Feb. 2019, doi: 10.1109/JPHOT.2019.2894300.

[58] A. C. Mishra, P. Lohia, and D. K. Dwivedi, "Long period grating based optical fiber sensors: Fabrication techniques and characteristics," in *Proc. Int. Conf. Electr. Electron. Eng. (ICE)*, Feb. 2020, pp. 49–52, doi: 10.1109/ICE348803.2020.9122964.

[59] F. Esposito, "Chemical sensors based on long period fiber gratings: A review," *Results Opt.*, vol. 5, Dec. 2021, Art. no. 100196, doi: 10.1016/j.rio.2021.100196.

[60] Y.-Q. Ni, S. Ding, B. Han, and H. Wang, "Layer-by-layer assembly of polyelectrolytes-wrapped multi-walled carbon nanotubes on long period fiber grating sensors," *Sens. Actuators B, Chem.*, vol. 301, Dec. 2019, Art. no. 127120, doi: 10.1016/j.snb.2019.127120.

[61] R. Y.-N. Wong, D. H. J. Juan, M. Ibsen, and P. P. Shum, "Optical fibre long-period grating sensors operating at and around the phase matching turning point," in *Applications of Optical Fibers for Sensing*. IntechOpen, Jan. 2019, doi: 10.5772/intechopen.81179.

[62] K. P. W. Dissanayake, W. Wu, H. Nguyen, T. Sun, and K. T. V. Grattan, "Graphene-oxide-coated long-period grating-based fiber optic sensor for relative humidity and external refractive index," *J. Lightw. Technol.*, vol. 36, no. 4, pp. 1145–1151, Feb. 15, 2018, doi: 10.1109/JLT.2017.2756097.

[63] N. Sahoo, Z. Sun, K. Zhou, X. Chen, Y. Tan, and L. Zhang, "Graphene-oxide coated LPGs for humidity sensing applications," *Proc. SPIE*, vol. 11355, Apr. 2020, Art. no. 1135505, doi: 10.1117/12.2555365.

[64] Y.-T. Tsai, C.-W. Wu, L. Tsai, and C.-C. Chiang, "Application of graphene oxide-based, long-period fiber grating for sensing relative humidity," *J. Lightw. Technol.*, vol. 39, no. 12, pp. 4124–4130, Jun. 15, 2021, doi: 10.1109/JLT.2020.3006380.

[65] M. Tian, Y. Huang, C. Li, and M. Lv, "High-performance humidity sensor based on a micro-nano fiber Bragg grating coated with graphene oxide," *Opt. Exp.*, vol. 28, no. 18, p. 26395, 2020, doi: 10.1364/oe.402648.

[66] F. Gu, H. Yu, W. Fang, and L. Tong, "Nanoimprinted polymer micro/nanofiber Bragg gratings for high-sensitivity strain sensing," *IEEE Photon. Technol. Lett.*, vol. 25, no. 1, pp. 22–24, Jan. 1, 2013, doi: 10.1109/LPT.2012.2227467.

[67] R. Rohan, K. Venkadeshwaran, and P. Ranjan, "Recent advancements of fiber Bragg grating sensors in biomedical application: A review," *J. Opt.*, vol. 1, pp. 1–12, Mar. 2023, doi: 10.1007/S12596-023-01134-9.

[68] J.-L. Kou, M. Ding, J. Feng, Y.-Q. Lu, F. Xu, and G. Brambilla, "Microfiber-based Bragg gratings for sensing applications: A review," *Sensors*, vol. 12, no. 7, pp. 8861–8876, Jun. 2012, doi: 10.3390/s120708861.

[69] V. Bhardwaj, K. Kishor, and A. C. Sharma, "Tapered optical fiber geometries and sensing applications based on Mach–Zehnder interferometer: A review," *Opt. Fiber Technol.*, vol. 58, Sep. 2020, Art. no. 102302, doi: 10.1016/j.yofte.2020.102302.

[70] X. Fan, S. Deng, Z. Wei, F. Wang, C. Tan, and H. Meng, "Ammonia gas sensor based on graphene oxide-coated Mach–Zehnder interferometer with hybrid fiber structure," *Sensors*, vol. 21, no. 11, p. 3886, Jun. 2021, doi: 10.3390/s21113886.

[71] X. Lei, X. Dong, T. Sun, and K. T. V. Grattan, "Ultrasensitive refractive index sensor based on Mach–Zehnder interferometer and a 40 μm fiber," *J. Lightw. Technol.*, vol. 39, no. 17, pp. 5625–5633, Sep. 1, 2021, doi: 10.1109/JLT.2021.3087037.

[72] N. F. Baharin, A. I. Azmi, A. S. Abdullah, and M. Y. M. Noor, "Refractive index sensor based on lateral-offset of coreless silica interferometer," *Opt. Laser Technol.*, vol. 99, pp. 396–401, Feb. 2018, doi: 10.1016/j.optlastec.2017.09.028.

[73] A. Miliou, "In-fiber interferometric-based sensors: Overview and recent advances," *Photonics*, vol. 8, no. 7, p. 265, Jul. 2021, doi: 10.3390/photonics8070265.

[74] S. Liu, H. Meng, S. Deng, Z. Wei, F. Wang, and C. Tan, "Fiber humidity sensor based on a graphene-coated core-offset Mach–Zehnder interferometer," *IEEE Sensors Lett.*, vol. 2, no. 3, pp. 1–4, Sep. 2018, doi: 10.1109/LSENS.2018.2849750.

[75] X. Fan, Q. Wang, M. Zhou, F. Liu, H. Shen, Z. Wei, F. Wang, C. Tan, and H. Meng, "Humidity sensor based on a graphene oxide-coated few-mode fiber Mach–Zehnder interferometer," *Opt. Exp.*, vol. 28, no. 17, p. 24682, Aug. 2020, doi: 10.1364/oe.390207.

[76] Z. Wang, L. Li, M. Wang, Q. Ma, Y. Lou, Q. Wu, and B. Peng, "Fiber core-offset humidity sensor based on graphene oxide characteristics," *IEEE Photon. J.*, vol. 13, no. 3, pp. 1–8, Jun. 2021, doi: 10.1109/JPHOT.2021.3083699.

[77] J. Fu, Y. Xu, M. Xu, L. G. Abbas, and A. Zhou, "Highly sensitive humidity sensor based on tapered dual side-hole fiber," *Optik*, vol. 261, Jul. 2022, Art. no. 169183, doi: 10.1016/j.ijleo.2022.169183.

[78] X. Ding, J. Yan, N. Chen, T. Jin, and R. Zhang, "Highly sensitive balloon-like fiber interferometer based on GO nanomaterial coated for humidity measurement," *Opt. Laser Technol.*, vol. 158, Feb. 2023, Art. no. 108798, doi: 10.1016/j.optlastec.2022.108798.

[79] G. P. Agrawal, "Fiber interferometers," in *Applications of Nonlinear Fiber Optics*, 3rd ed. Academic, Jan. 2021, pp. 109–141, doi: 10.1016/B978-0-12-817040-3.00009-2.

[80] X. Liu, B. Jin, Q. Bai, Y. Wang, D. Wang, and Y. Wang, "Distributed fiber-optic sensors for vibration detection," *Sensors*, vol. 16, no. 8, p. 1164, Jul. 2016, doi: 10.3390/s16081164.

[81] A. D. Gomes, H. Bartelt, and O. Frazão, "Optical Vernier effect: Recent advances and developments," *Laser Photon. Rev.*, vol. 15, no. 7, Jul. 2021, Art. no. 2000588, doi: 10.1002/lpor.202000588.

[82] B. H. Lee, Y. H. Kim, K. S. Park, J. B. Eom, M. J. Kim, B. S. Rho, and H. Y. Choi, "Interferometric fiber optic sensors," *Sensors*, vol. 12, no. 3, pp. 2467–2486, Feb. 2012, doi: 10.3390/s120302467.

[83] R. Chu, C. Guan, Y. Bo, J. Shi, Z. Zhu, P. Li, J. Yang, and L. Yuan, "All-optical graphene-oxide humidity sensor based on a side-polished symmetrical twin-core fiber Michelson interferometer," *Sens. Actuators B, Chem.*, vol. 284, pp. 623–627, Apr. 2019, doi: 10.1016/j.snb.2019.01.011.

[84] L. Gai, J. Li, and Y. Zhao, "Preparation and application of microfiber resonant ring sensors: A review," *Opt. Laser Technol.*, vol. 89, pp. 126–136, Mar. 2017, doi: 10.1016/j.optlastec.2016.10.002.

[85] H. Dang, M. Chen, J. Li, and W. Liu, "Sensing performance improvement of resonating sensors based on knotting micro/nanofibers: A review," *Measurement*, vol. 170, Jan. 2021, Art. no. 108706, doi: 10.1016/j.measurement.2020.108706.

[86] S. R. Azzuhri, I. S. Amiri, A. S. Zulkhairi, M. A. M. Salim, M. Z. A. Razak, M. F. Khyasudeen, H. Ahmad, R. Zakaria, and P. Yupapin, "Application of graphene oxide based microfiber-knot resonator for relative humidity sensing," *Results Phys.*, vol. 9, pp. 1572–1577, Jun. 2018, doi: 10.1016/j.rinp.2018.05.009.

[87] Y.-G. Han, "Relative humidity sensors based on microfiber knot resonators—A review," *Sensors*, vol. 19, no. 23, p. 5196, Nov. 2019, doi: 10.3390/s19235196.

[88] R. Zhao, J. Cui, Y. Yu, X. Zhai, X. Chu, M. Zhu, B. Wu, Y. Yang, R. Wang, C. He, G. Zhang, and W. Zhang, "Research on acoustic sensing device based on microfiber knot resonator," *J. Micromech. Microeng.*, vol. 32, no. 8, Aug. 2022, Art. no. 085003, doi: 10.1088/1361-6439/ac7842.
[89] M. J. Faruki, M. Z. Ab Razak, S. Azzuhri, M. T. Rahman, M. R. K. Soltanian, G. Brambilla, B. M. A. Rahman, K. V. Grattan, R. De La Rue, and H. Ahmad, "Effect of titanium dioxide (TiO_2) nanoparticle coating on the detection performance of microfiber knot resonator sensors for relative humidity measurement," *Mater. Exp.*, vol. 6, no. 6, pp. 501–508, Dec. 2016, doi: 10.1166/mex.2016.1342.
[90] Y. Peng, Y. Zhao, M. Chen, and F. Xia, "Research advances in microfiber humidity sensors," *Small*, vol. 14, no. 29, Jul. 2018, Art. no. 1800524, doi: 10.1002/smll.201800524.
[91] V. A. Nebol'sin, V. Galstyan, and Y. E. Silina, "Graphene oxide and its chemical nature: Multi-stage interactions between the oxygen and graphene," *Surf. Interfaces*, vol. 21, Dec. 2020, Art. no. 100763, doi: 10.1016/j.surfin.2020.100763.
[92] C.-Y. Huang, Y.-C. Lin, J. H. Y. Chung, H.-Y. Chiu, N.-L. Yeh, S.-J. Chang, C.-H. Chan, C.-C. Shih, and G.-Y. Chen, "Enhancing cementitious composites with functionalized graphene oxide-based materials: Surface chemistry and mechanisms," *Int. J. Mol. Sci.*, vol. 24, no. 13, p. 10461, Jun. 2023, doi: 10.3390/ijms241310461.
[93] O. C. Compton and S. T. Nguyen, "Graphene oxide, highly reduced graphene oxide, and graphene: Versatile building blocks for carbon-based materials," *Small*, vol. 6, no. 6, pp. 711–723, Mar. 2010, doi: 10.1002/smll.200901934.
[94] A. Blank and Y. Linzon, "Optimizing contact area geometry and taper composition in microknot resonators," *J. Appl. Phys.*, vol. 125, no. 23, Jun. 2019, Art. no. 233103, doi: 10.1063/1.5093070.
[95] H. A. Zain, M. H. Jali, H. R. A. Rahim, M. A. M. Johari, H. H. M. Yusof, S. Thokchom, M. Yasin, and S. W. Harun, "ZnO nanorods coated microfiber loop resonator for relative humidity sensing," *Opt. Fiber Technol.*, vol. 54, Jan. 2020, Art. no. 102080, doi: 10.1016/j.yofte.2019.102080.
[96] W. Luo, Y. Chen, and F. Xu, "Recent progress in microfiber-optic sensors," *Photonic Sensors*, vol. 11, no. 1, pp. 45–68, Mar. 2021, doi: 10.1007/s13320-021-0614-9.
[97] N. Irawati, H. A. Rahman, H. Ahmad, and S. W. Harun, "A PMMA microfiber loop resonator based humidity sensor with ZnO nanorods coating," *Measurement*, vol. 99, pp. 128–133, Mar. 2017, doi: 10.1016/j.measurement.2016.12.021.
[98] H. Hamrayev, K. Shameli, and M. Yusefi, "Preparation of zinc oxide nanoparticles and its cancer treatment effects: A review paper," *J. Adv. Res. Micro Nano Eng.*, vol. 2, no. 1, pp. 1–11, Dec. 2020. Accessed: Aug. 10, 2023. [Online]. Available: https://www.akademiabaru.com/submit/index.php/armne/article/view/2962
[99] E. Wongrat, N. Chanlek, C. Chueaiarrom, B. Samransuksamer, N. Hongsith, and S. Choopun, "Low temperature ethanol response enhancement of ZnO nanostructures sensor decorated with gold nanoparticles exposed to UV illumination," *Sens. Actuators A, Phys.*, vol. 251, pp. 188–197, Nov. 2016, doi: 10.1016/j.sna.2016.10.022.
[100] F. Wang, B. Wang, X. Zhang, M. Lu, Y. Zhang, C. Sun, and W. Peng, "High sensitivity humidity detection based on functional GO/MWCNTs hybrid nano-materials coated titled fiber Bragg grating," *Nanomaterials*, vol. 11, no. 5, p. 1134, Apr. 2021, doi: 10.3390/nano11051134.

SITI NASUHA MUSTAFFA received the B.Sc. degree (Hons.) in applied physics from the Islamic Science University of Malaysia (USIM), Nilai, Negeri Sembilan, Malaysia, in 2022. She is currently pursuing the M.S degree in microengineering and nanoelectronics with the Institute of Microengineering and Nanoelectronics (IMEN), UKM. Her current research focuses on tapered optical fiber sensor for refractive index sensing.

AFFA ROZANA ABDUL RASHID received the B.Eng. degree (Hons.) in electric, electronics and system engineering and the M.Sc. degree in microelectronics from the National University of Malaysia [Universiti Kebangsaan Malaysia (UKM)], Bangi, Malaysia, in 2008 and 2009, respectively, and the Ph.D. degree from the Institute of Microengineering and Nanoelectronics (IMEN), UKM, where she focused on fiber optic sensors. Since 2014, she has been a Senior Lecturer and became the Head (in 2021) of the Applied Physics Program, Faculty of Science and Technology, Universiti Sains Islam Malaysia (USIM). She specializing in the field of plasmonics, nanophotonics, optoelectronics, and fiber optic sensors. She is a member of the IEEE Electron Devices Society, the IEEE Photonics Society, and the Malaysian Solid State Science and Technology Society (MASS); and a Registered Engineer with the Board of Engineers Malaysia (BEM). In 2017, she received the Excellent Service Award (APC) from USIM for her contribution. She has participated actively in innovation and achieved Gold Award at International Conference and Exposition on Inventions by Institutions of Higher Learning (PECIPTA 2022), Malaysia Technology Expo (MTE 2022), and EduNovation: Transformation Toward Entrepreneurial Mindset (EdNovaC 2019). She was an Editor of *Malaysian Journal of Science, Health and Technology* (MJoSHT) and *Nano Hybrids and Composites*.

TAN SIN JIN received the Engineering degree from University Teknologi Malaysia, and the M.E. and Ph.D. degrees from the University of Malaya. She is currently a Senior Lecturer with the School of Engineering, UOW Malaysia. She is registered as a Professional Engineer under the Board of Engineer Malaysia. Her research interests include photonics, optical, and electronics systems.

P. SUSTHITHA MENON (Senior Member, IEEE) received the B.Eng. (Hons.) and M.Sc. degrees in microelectronics from the National University of Malaysia (UKM), in 1998 and 2005, respectively, and the Ph.D. degree (Hons.) in optoelectronics from the Institute of Microengineering and Nanoelectronics (IMEN), UKM, in 2008, researching on InGaAs/InP p-i-n photodiodes. She was attached to Intel Malaysia, as a Product Engineer, from 1999 to 2002, during which she was a New Product Integration (NPI) Engineer with the Intel's Systems Manufacturing Technology Division (SMTD), Oregon, USA. She joined IMEN, as a Postdoctoral Fellow, in 2008, and worked on the development of GaAs/InP-based long-wavelength vertical-cavity surface emitting lasers (LW-VCSELs). Since 2009, she has been a Senior Research Fellow with IMEN. She is the author of four book chapters, more than 200 indexed articles, and four patents. Her current research interests include plasmonics, optoelectronics, nanophotonics, and engineering optimization. She is the Chair of the Women in Electron Devices Society (WiEDS), a member of the IEEE Electron Devices Society (EDS) Board of Governors (BoG) and the past Chair of the IEEE EDS Malaysia Chapter.

MOHD ZULHAKIMI AB RAZAK received the B.Eng. degree (Hons.) in electronics and electrical engineering from the University of Strathclyde, U.K., the M.Eng.Sc. degree in electronics and information technology from the University of Applied Science Rosenheim, Germany, and the Ph.D. degree from The University of Edinburgh, U.K. His Ph.D. thesis focused on smart circuit design strategies and adaptive integrated circuit (IC) design for wireless applications. He is currently a Research Fellow with the Institute of Microengineering and Nanoelectronics (IMEN), Universiti Kebangsaan Malaysia (UKM), Malaysia. His research interests include integrated system design, optoelectronics systems, mixed-signal IC design, and smart circuits for Internet of Things (IoT) applications.

ARNI MUNIRA MARKOM received the bachelor's degree in electronics engineering (computer engineering), in 2007, the master's degree in microelectronics, in 2009, and the Ph.D. degree in electronics (photonics engineering), in 2016. She is a highly accomplished Senior Lecturer with the School of Electrical Engineering, College of Engineering, Universiti Teknologi MARA, Shah Alam, Malaysia. Her research focuses on photonics technology, fiber lasers, fiber sensors, embedded systems, and IoT devices. She has made significant contributions to her field. Her research expertise and dedication have earned her several prestigious awards, including the Industrial Linkage Excellent Award, in 2021; the UiTM Top Talent Award (South Zone), in 2021; and the title of Promising Academic Member, in 2021. Furthermore, she was recognized as the Best Writer for 2020 and received the Excellence Service Award, in 2019, for her outstanding written contributions and exceptional service. Her potential as a researcher was acknowledged with the Most Promising Researcher Award, in 2019, highlighting her impact and potential within the research community. She actively collaborates with industry partners and academic institutions to drive innovation and practical applications.

HAZLIHAN HARIS was born in Sabah, Malaysia. He received the bachelor's degree (Hons.) in electrical engineering, majoring in electrical, the master's degree in photonic engineering, and the Ph.D. degree in electrical engineering (photonics) from the University of Malaya, Malaysia, in 2012, 2014, and 2018, respectively. He is currently a Postdoctoral Researcher with the Faculty of Engineering, Universiti Malaysia Sabah. His current research focusing on the generation of ultrafast laser by incorporating 2-D nanomaterials as passive saturable absorber. He is registered as a Graduate Engineer with the Board of Engineering Malaysia (BEM), in 2013.

ISMAIL SAAD (Senior Member, IEEE) received the B.Eng. degree (Hons.) in electronics/computer engineering from University Putra Malaysia (UPM), in 1999, the M.Sc. degree in microelectronics system design from the University of Southampton, U.K., in 2001, and the Ph.D. degree specializing in micro and nanoelectronics device and material from University Technology Malaysia (UTM), in 2009. He has been a full-time Lecturer with Universiti Malaysia Sabah (UMS), since 2002, and was promoted as an Associate Professor. He is lecturing in the area of VLSI technology and design, microprogramming, microprocessors, and semiconductor device. He has held a positions of the Dean of the Faculty of Engineering, the Director of the Artificial Intelligent Research Unit, and the Program Head of electrical and electronics engineering and the business and innovation with the UMS Centre of Co-Curriculum and Student Development. He demonstrates active involvement in administration. His enthusiasm for research and securing RM1.5 million in research grants with numerous devoted collaborative research partners. He has been a Graduate Member of the Board of Engineer Malaysia (BEM), since 1999, and the Institute of Engineers Malaysia (IEM), since 2010. He has been an Active Member of IEEE, since 2007. During his Ph.D. Convocation Ceremony, he received the Chancellor Award and the Best Student Award for his excellent academic achievements.

AHMAD RAZIF MUHAMMAD received the B.Eng. degree (Hons.) in mechanical engineering, the M.Phil. degree in photonics engineering, and the Ph.D. degree in electrical engineering (photonics) from the University of Malaya. His Ph.D. thesis focused on short pulse fiber laser based on pure metal saturable absorber. Currently, he is a Research Fellow with the Institute of Microengineering and Nanoelectronics (IMEN), Universiti Kebangsaan Malaysia (UKM), Malaysia. His research interests include NIR fiber laser, ultrafast fiber laser, and nanofiber for optical sensing.